Electron Paramagnetic Resonance Studies of a System with Orbital Degeneracy: The Lithium Donor in Silicon

G. D. WATKINS AND FRANK S. HAM
General Electric Research and Development Center, Schenectady, New York 12301
(Received 1 December 1969)

Electron-paramagnetic-resonance (EPR) and electron-nuclear double-resonance (ENDOR) spectra are reported for the first time for the isolated interstitial lithium shallow-donor center in silicon. In zero applied stress the EPR spectrum is complicated because of the fivefold orbital degeneracy (doublet E+triplet T_2) of the donor ground state which results from the inverted valley-orbit splitting (singlet A_1 higher by 1.8 meV). Below 2.5°K this spectrum contains a number of strongly anisotropic lines, the effective g values of which are all $\gtrsim 2.000$ at the experimental frequencies $\nu_0=10$, 14, and 20 kMc/sec and vary linearly in ν_0^{-2}. This spectrum is extremely sensitive to small applied stresses; its structure simplifies above 2.5°K as a result of relaxation effects. These features may be accounted for by postulating a very weak spin-orbit interaction (in the range ~ 0.01 to ~ 0.05 cm^{-1}) among the T_2 states and between the E and T_2 states. Also, splittings of these states caused by random crystal strains [$(\sim 1$–$2)\times 10^{-6}$] in our samples must be larger than the spin-orbit splitting but smaller than $h\nu_0$. Under strong uniaxial compression along [001] or tension along [110], the EPR spectrum simplifies to a single line having axial symmetry about [001] with $g_{\parallel}=1.9997\pm 0.0001$, $g_{\perp}=1.9987\pm 0.0001$, in agreement now with the predictions of the independent-valley model for a nondegenerate ground state representing the antisymmetric combination of valleys on the z axis. ENDOR spectra of Li^7, Li^6, and Si^{29} have been observed under these stress conditions in the range 1.3–4°K and are interpreted in terms of a lifetime-averaged hyperfine interaction of the T_2z ground state and the lowest excited electronic state (which represents the symmetric combination of the z valleys in the limit of large stress). The Li^7 hyperfine interaction is found to vary from $A/h\simeq 0.01$ Mc/sec at 1.3°K to ~ 0.10 Mc/sec at 4°K, from which data a value $A_0/h=2.3\pm 0.5$ Mc/sec is inferred for the hyperfine interaction of the excited singlet state in zero stress. The various parameters of the experimental spectrum are interpreted in terms of effective-mass theory, augmented by the spin-orbit interaction and other necessary refinements of our theoretical model. The EPR data show that the lithium is definitely not in the hexagonal interstitial site, but rather is in the tetrahedral site (or possibly slightly displaced from the tetrahedral site). Analysis of stress dependence of the EPR and ENDOR data gives a value $\Xi_u=+11.4\pm 1.1$ eV for the deformation-potential parameter of the conduction-band minima.

I. INTRODUCTION

THE shallow donors in silicon are among the most extensively studied and best understood impurity centers of solid-state physics. Their electronic structure, worked out on the basis of effective-mass theory,[1] has been confirmed in considerable detail from studies of their electron-paramagnetic-resonance (EPR) and electron-nuclear double-resonance (ENDOR) spectra.[2] These studies have been especially fruitful for the substitutional donors phosphorus, arsenic, and antimony, particularly through the investigations of Feher and his colleagues.[3–5] For the interstitial lithium donor, in contrast, no EPR spectrum has previously been reported,[6] although of all the shallow donors in silicon, lithium has a binding energy[7] closest to that predicted by simple uncorrected effective-mass theory. One might therefore expect the predictions of effective-mass theory to be even more closely fulfilled for other properties of this center than they are for the other donors. The purpose of this paper is to describe the unusual EPR and ENDOR spectra of the isolated lithium atom in silicon which we have now identified and have studied in some detail, and to propose a theoretical interpretation which accounts for the main features of these spectra.

A spin resonance originally attributed to the lithium donor was first observed by Honig and Kip[8] in crucible-grown silicon and subsequently studied by Feher.[3] Feher found, however, that this resonance was absent when floating-zone silicon was used, and he suggested that it arose from a lithium-oxygen complex rather than from the isolated lithium center. Aggarwal *et al.*,[7] confirming that different centers were involved in the two types of silicon, showed that the lithium-oxygen complex in crucible-grown silicon has an altogether different far-infrared excitation spectrum from that of the isolated lithium in the floating-zone material. Uniaxial-stress experiments showed that the spectrum of the lithium-oxygen complex behaved similarly to that of the substitutional donors, for which the valley-orbit splitting leaves the ground state an orbital singlet. From the

[1] A comprehensive review of effective-mass theory as applied to the shallow impurity states in silicon and germanium, and of the experimental work that led to this development, is given in the article by W. Kohn, in *Solid State Physics*, edited by F. Seitz and D. Turnbull (Academic, New York, 1957), Vol. 5, p. 257.

[2] Reviews of the earlier EPR and ENDOR work in semiconductors are given in the article by G. W. Ludwig and H. H. Woodbury, in *Solid State Physics*, edited by F. Seitz and D. Turnbull (Academic, New York, 1962), Vol. 13, p. 223, and in the monograph by G. Lancaster, *Electron Spin Resonance in Semiconductors* (Plenum, New York, 1967).

[3] G. Feher, Phys. Rev. **114**, 1219 (1959).

[4] G. Feher and E. A. Gere, Phys. Rev. **114**, 1245 (1959).

[5] D. K. Wilson and G. Feher, Phys. Rev. **124**, 1068 (1961).

[6] A preliminary report of the present work was given by G. D. Watkins, Bull. Am. Phys. Soc. **10**, 303 (1965).

[7] R. L. Aggarwal, P. Fisher, V. Mourzine, and A. K. Ramdas, Phys. Rev. **138**, A882 (1965).

[8] A. Honig and A. F. Kip, Phys. Rev. **95**, 1686 (1954).

stress splitting of the lithium spectrum, however, Aggarwal *et al.* concluded that for the isolated lithium the valley-orbit splitting is inverted, the ground state having a fivefold orbital degeneracy (or near degeneracy) comprising the doublet and triplet valley-orbit states, with the singlet some 1.8 meV higher. The absence of the simple spin resonance found for the donors having the "normal" sign of the valley-orbit splitting was therefore apparently a consequence of having this additional degeneracy in the ground state.

The EPR spectrum which we have now identified as due to the isolated lithium is indeed complicated as a result of this orbital degeneracy in the ground state, but in a rather unexpected way. Because of the complicated nature of the experimental spectrum, we have found it necessary to rely heavily on the theory in sorting out the data, and in turn, the unusual features of the data have dictated the direction in which the theory had to be developed. In view of the close interweaving of theory and experiment, we have adopted in this paper a presentation which alternates between the description of the experimental results and the development of the necessary theoretical framework. Since the predictions of simple effective-mass theory as regards the EPR spectrum to be expected for the inverted valley-orbit splitting have never been fully developed, we begin, after a short description in Sec. II of our experimental procedures, by working out in Sec. III the consequences of this simple theory for the doublet and triplet states. Here we use the independent-valley model, which has been shown by Feher[3] and by Wilson and Feher[5] to account successfully for the EPR and ENDOR spectra of the substitutional donors, but we must take into account the special effects of random strain and relaxation, which are of particular importance for the doublet spectrum. We also consider here the predictions of the simple theory for the effect of an applied uniaxial stress.

In Sec. IV we describe the general features of the experimental spectra, with and without an applied stress. We show that, whereas the simple theory of Sec. III fails entirely to provide any explanation for the most prominent features of the spectrum in zero stress, the data do conform to this theory when a sufficiently large stress (of the appropriate sense) is applied to completely remove the orbital degeneracy in the ground state. We examine this latter case, for which the state corresponding to the antisymmetric combination of valleys along a single axis is lowest, in detail in Sec. V. Not only the antisotropic g factor but also the EPR linewidth resulting from the Si^{29} hyperfine interaction are shown to be described quite well by the effective-mass theory. The results of ENDOR experiments under stress are described for both the lithium (Li^6 and Li^7) and Si^{29} nuclei and accounted for in terms of the theory.

We return in Sec. VI to consideration of the zero-stress EPR spectrum, where we show that its unusual features can be explained if we postulate a very weak spin-orbit interaction among the doublet and triplet valley-orbit states. The theory for this situation is first developed in detail to derive the anisotropy of the predicted resonances both for zero stress and for an applied stress that only partially lifts the orbital degeneracy, and these theoretical results are then compared with the experimental data. It is shown that this model also accounts qualitatively for the unusual behavior of the EPR spectrum under small applied stress. The crucial role played by the splittings due to random crystal strains is discussed, along with the limitations on the applicability of the theory which are thereby imposed. The origin of the spin-orbit interaction, which of course is outside the framework of the independent-valley model, is then considered and shown to lie with the silicon spin-orbit interaction of the crystal rather than in a residual effect of the lithium atomic impurity. We also show that the EPR data may be used to determine the site symmetry of the interstitial lithium ion, and we thereby conclude that the site is definitely not the hexagonal site suggested by Weiser[9] from his consideration of lithium's high diffusion rate in silicon, but rather the tetrahedral site (although there remains a possibility that the lithium is displaced slightly out of the tetrahedral site).

Electron paramagnetic resonance in other systems with orbital degeneracy is known to involve very important vibronic effects, notably the Jahn-Teller effect in its dynamic and static manifestations.[10,11] We conclude Sec. VI by discussing how such effects would affect the lithium spectrum if they were significant. We conclude, on the basis of the theoretical considerations of the coupling strength for Jahn-Teller interactions for shallow donors and from the evidence of the experimental data, that despite the orbital degeneracy of the ground state of the lithium donor such effects are of no importance for the interpretation of the EPR spectrum.

Section VII completes our analysis with a more detailed consideration of the stress dependence of the spectrum, which we use to obtain from our data a value for the deformation potential parameter Ξ_u. This is compared with other determinations. A concluding summary is given in Sec. VIII.

The lithium spectrum poses a challenging problem, both experimental and theoretical, because of the unusual features which it reveals. Its novelty may be given particular emphasis by contrasting it in two important respects with familiar EPR and ENDOR systems. First, for the lithium donor the relative order of the effective crystal-field, spin-orbit, and Zeeman interactions is reversed from the usual one, in that the Zeeman splitting in typical magnetic fields here is larger than

[9] K. Weiser, Phys. Rev. **126**, 1427 (1962).
[10] F. S. Ham, Phys. Rev. **138**, A1727 (1965).
[11] An article reviewing the theory of dynamic Jahn-Teller effects in EPR spectra is scheduled for publication in 1970: F. S. Ham, in *Electron Paramagnetic Resonance*, edited by S. Geschwind (Plenum, New York, 1970).

both the crystal-field splitting (e.g., the splitting of the orbital degeneracy due to random strain, as well as the separation of the doublet and triplet states in zero stress) and the even smaller spin-orbit interaction. Second, in the ENDOR studies under stress, the lithium hyperfine interaction is found to vary continuously by one order of magnitude as the temperature is changed from 1.3 to 4°K. As will be shown in Sec. V, this remarkable temperature variation is the result of a nearly vanishing hyperfine interaction in the ground state and of a lifetime averaging that persists even at these low temperatures because of the short lifetime and very small excitation energy of an excited state of the electronic system. In these two respects, the isolated lithium in silicon is to the best of our knowledge unique among systems on which EPR and ENDOR studies have been made.

II. EXPERIMENTAL PROCEDURE

Most of the lithium-doped samples were supplied to us by A. K. Ramdas. His procedure for lithium doping has been previously described[7,12] and involves a 30-min in-diffusion of lithium at 400°C followed after surface cleaning by a 2-h 600°C treatment to insure homogeneous distribution of the lithium. Both enriched Li^6 and normal isotopic abundance samples were prepared. The starting material was commercially avialable undoped vacuum floating-zone single-crystal silicon. The resulting concentration of lithium measured by electrical resistivity was $\sim 10^{16}/cm^3$. A few samples were also prepared in our laboratory following his recipe.

Before lithium diffusion, oversize samples ($\sim$0.125 in. $\times$0.125 in.$\times$0.900 in.) were cut with the long dimension oriented (within $\sim 2°$) along the desired crystallographic direction. After doping, the samples were oriented by x-ray back-reflection Laue techniques *in situ* on a precision surface grinder and all surfaces ground and squared off to the desired final dimensions ($\sim$0.090 in. $\times$0.090 in.$\times$0.850 in.). In this way the orientation of the long dimension of the crystal was kept within ~ 10 sec of arc of the desired crystallographic direction.

The two ends of the sample were tinned with indium, using an ultrasonic soldering gun, and then indium-soldered into brass cups. These cups in turn could be screwed into phosphor-bronze universal joints above and below (and coaxial with) the TE_{011} microwave cavity as shown in Fig. 1. The lower universal joint was supported by the cavity assembly so that by pushing or pulling on the rod connected to the upper universal joint, uniaxial compression or tension could be applied to the sample. The universal joints were carefully cleaned of all greases and oils that might freeze at cryogenic temperatures, and lubrication was achieved by dusting the joints with MoS_2. This arrangement provided uniaxial stress to the sample, virtually free of unwanted off-axis components, even though the cavity assembly might flex somewhat under the applied stress. The samples were long enough so that only the sample was in the cavity proper. The rod was brought out of the cryostat assembly through an O ring, and stresses were applied externally by a simple lever and weights.

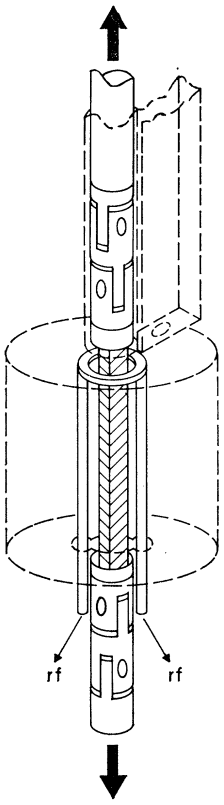

FIG. 1. Universal joint assembly used to supply uniaxial stress to the sample in the TE_{011} microwave cavity. Also shown is the single-turn ENDOR coil.

With the vertical stress geometry of Fig. 1, the dc magnetic field **H** is confined to the plane perpendicular to the stress directions. Most of the studies were limited to this configuration. One experiment was performed in which a horizontal compressional stress could be applied, allowing **H** to be oriented along the stress direction. This was performed in the 10-kMc/sec EPR spectrometer of Tucker. The special cavity assembly that he has designed for this purpose has been previously described.[13]

Most of the EPR studies were performed on a balanced bolometer system operating at 20 kMc/sec. For most of the experiments also, conventional 94-cps magnetic field modulation was used with lock-in detection and recording. The relaxation times were short enough at all temperatures studied that derivative of dispersion or absorption curves were recorded.

For some experiments it was necessary to keep track of the intensities in various parts of the spectrum, and for these it was desirable to record absorption directly.

[12] E. M. Pell, in *Solid State Physics in Electronics and Telecommunications*, edited by M. Desirant and J. L. Michiels (Academic, New York, 1960), Vol. 1, p. 261.

[13] E. B. Tucker, Phys. Rev. **143**, 264 (1966).

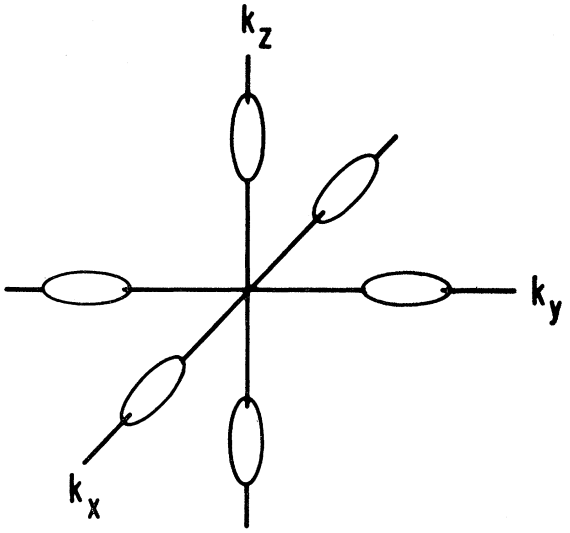

FIG. 2. Constant-energy ellipsoids associated with the six conduction-band minima in silicon.

In order to do this, the microwave power going to the cavity was on-off square-wave amplitude modulated at 94 cps by supplying a square wave of current to a commercially available ferrite modulator.[14] By carefully matching the cavity to the waveguide and balancing the spectrometer, it was possible to reduce the detected 94-cps signal off-resonance to zero. On resonance, the detected 94-cps signal was therefore directly proportional to the absorption. Conventional 94-cps lock-in detection and recording techniques were then used to plot out the absorption signal. With care in rigidly supporting the microwave components, avoiding drafts, etc., it was possible to maintain the spectrometer balance sufficiently well, so that after a few hours warmup the spectrum could be recorded with negligible baseline drift and with signal-to-noise ratio comparable to that achieved with magnetic field modulation techniques.

Limited studies were also performed at 14 and 10 kMc/sec. These were with conventional magnetic field modulation, and stress for these experiments was applied via a rod to the sample, the other end of which was soldered to the base of the cavity.

ENDOR studies were achieved via a single-turn coil, inside the microwave cavity, as shown in Fig. 1. (The loop in the upper end of the coil serves the purpose only of allowing the entry of the sample. The functional parts of the coil are the vertical rods, the resulting rf magnetic field being perpendicular to the axis of the cavity.) The rf current was supplied to the coil from a General Radio 1211B unit oscillator via a Hewlett-Packard 460 BR-distributed amplifier. Square-wave on-off amplitude modulation of the rf current was achieved by applying a 94-cps square wave as grid bias to the distributed amplifier tubes. No magnetic field modulation was used, therefore, in the ENDOR studies, and 94-cps lock-in detection and recording were used as the frequency of the rf signal was swept.

[14] Model K-212 gyraline, manufactured by Cascade Research Corp.

III. BASIC THEORY

A. Electronic Structure

The theory of the shallow donor states in silicon has been developed by Luttinger and Kohn[15] and has been reviewed by Kohn.[1]

In the treatment of Luttinger and Kohn, the electron wave functions of shallow donor states in silicon take the form

$$\Psi(\mathbf{r})=\sum_j \alpha_j \chi_j(\mathbf{r}), \tag{1}$$

where $\chi_j(\mathbf{r})$ is defined as

$$\chi_j(\mathbf{r})=F_j(\mathbf{r})u_j(\mathbf{r})\exp(i\mathbf{k}_0{}^j\cdot\mathbf{r}). \tag{2}$$

Here $u_j(\mathbf{r})\exp(i\mathbf{k}_0{}^j\cdot\mathbf{r})$ denotes the Bloch function[16] at the jth minimum of the conduction band located at $\mathbf{k}_0{}^j$, and $F_j(\mathbf{r})$ is an envelope function satisfying the effective-mass equation for the jth valley. For the purposes of this paper, $F_j(\mathbf{r})$ will always be the s-like hydrogenic ground-state wave function appropriate to the attractive Coulomb potential of the Li^+ impurity since in this work we are concerned with paramagnetic resonance only in states which can be constructed from this lowest-energy solution of the effective-mass equation for each valley. There are six minima (see Fig. 2) in the conduction band of silicon, located at the points $[k_0,0,0]$, $[-k_0,0,0],\ldots,[0,0,-k_0]$, with $k_0/k_{\max}\simeq 0.85$,[3] where $k_{\max}=(2\pi/a_0)$, and a_0 is the lattice constant. Labeling these minima, respectively, with $j=1,\ldots,6$, we have six independent states of the form of Eq. (1) derived from these ground-state effective-mass wave functions. The corresponding values for α_j in Eq. (1) for the combinations of these states belonging to the irreducible representations of the symmetry group T_d of the tetrahedron are

$$\begin{aligned}
&A_1 \quad \alpha_j=(1/\sqrt{6})(1,1,1,1,1,1),\\
&E\theta \quad \alpha_j=(1/\sqrt{12})(-1,-1,-1,-1,2,2),\\
&E\epsilon \quad \alpha_j=\tfrac{1}{2}(1,1,-1,-1,0,0),\\
&T_2x \quad \alpha_j=(1/\sqrt{2})(1,-1,0,0,0,0),\\
&T_2y \quad \alpha_j=(1/\sqrt{2})(0,0,1,-1,0,0),\\
&T_2z \quad \alpha_j=(1/\sqrt{2})(0,0,0,0,1,-1).
\end{aligned} \tag{3}$$

We have labeled these states to denote their transforma-

[15] J. M. Luttinger and W. Kohn, Phys. Rev. **97**, 869 (1955).

[16] The otherwise arbitrary phases of the Bloch functions are chosen to make $u_j(\mathbf{r})\exp(i\mathbf{k}_0{}^j\cdot\mathbf{r})$ real and positive at the site of the interstitial lithium ion, and we will assume in our analysis that this site has tetrahedral symmetry. This choice fixes the relative phases of the Bloch functions from the six minima in such a way that the linear combinations indicated in Eqs. (1) and (3) transform as indicated under the symmetry operations of T_d with respect to the lithium site.

tion properties under the group T_d, using the notation[17] of Mulliken.[18] Thus the states labeled T_2x, T_2y, T_2z transform under T_d as x, y, z, respectively, and belong to the representation T_2, and those labeled $E\theta$, $E\epsilon$ transform, respectively, as $(3z^2-r^2)$ and $\sqrt{3}(x^2-y^2)$ and belong to the representation E.

Although to the accuracy of the effective-mass approximation the six states [Eq. (3)] all have the same energy, the inadequacy of this approximation near the donor impurity ("central-cell corrections") may lift this degeneracy. If the impurity is at a site of tetrahedral symmetry, the two states of the doublet E according to group theory must remain degenerate, and similarly, the three states of the triplet T_2, but the singlet, doublet, and triplet may have different energies ("valley-orbit" or "chemical" splitting). Of course, if the site symmetry is lower than tetrahedral, the degeneracy may be further reduced. The substitutional donors P, Sb, and As have for the ground state the singlet; the triplet is higher by 11.7, 9.9, and 21.1 meV, respectively, while the doublet lies above the triplet by 1.35, 2.5, and 1.4 meV.[19] However, for Li in floating-zone silicon, Aggarwal *et al.*[7] concluded that the valley-orbit splitting is inverted, the ground state comprising the five states of the doublet and triplet (degenerate to within the experimental accuracy of $\sim$0.1 meV for the far-infrared optical measurements), with the singlet 1.8 ± 0.1 meV higher. The inverted splitting has been attributed by Nara and Morita[20] to the result of requiring that the singlet wave function be orthogonal to the $1s$ core states of the interstitial Li ion. Thus in EPR studies of Li in floating-zone silicon we are concerned at liquid-helium temperatures with the resonance spectrum arising from this orbitally degenerate (or near-degenerate) ground state, in contrast to the familiar situation encountered for P, Sb, and As donors in which the low-temperature EPR spectrum is that of the singlet.

B. Independent-Valley Model for EPR Spectrum

Here we consider the simple model in which the spin Zeeman interaction is given solely by the sum of the individual contributions of each of the constituent valleys. This model was found by Feher[3] and Wilson and Feher[5] to account satisfactorily for the EPR spectrum of the singlet ground state of the substitutional donors in silicon. We therefore extend this treatment to explore the predicted EPR spectrum for interstitial lithium.

The spin Zeeman interaction for shallow donor states of the form (1), as given by Roth[21] and Hasegawa[22] taking account of the effect on the Bloch functions of spin-orbit interaction in the silicon lattice, may be expressed as

$$\mathcal{H}_H=\beta\sum_{\alpha,\beta}\left[g_\perp\delta_{\alpha\beta}+(g_\parallel-g_\perp)\sum_j \mathcal{P}_j n_\alpha{}^j n_\beta{}^j\right]S_\alpha H_\beta. \quad (4)$$

Here $\mathbf{S}$ is the electron spin, $\mathbf{H}$ the applied magnetic field, $n_\alpha{}^j$ the α component of a unit vector pointed along the symmetry axis of the jth valley (which coincides for silicon with the $\langle 100\rangle$ axis on which the valley is situated), $\mathcal{P}_j$ the projection operator $|\chi_j\rangle\langle\chi_j|$ for the state $\chi_j(\mathbf{r})$ in Eq. (2), and $\beta=(e\hbar/2mc)$ the Bohr magneton. The axially symmetric g tensor for an electron in the jth valley is then given by the diagonal matrix element $\langle j|\mathcal{H}_H|j\rangle$ of Eq. (4) with respect to the state (2). The two components $g_\parallel$ and $g_\perp$ of this g tensor differ from the free-electron g value by a small amount (of order $2\text{–}4\times10^{-3}$), as a result of the silicon spin-orbit interaction.[21,22] Among the states of Eq. (3), the diagonal matrix element of $\mathcal{H}_H$ with respect to the singlet state A_1 yields the familiar isotropic g factor for the singlet:

$$g_0=\tfrac{1}{3}g_\parallel+\tfrac{2}{3}g_\perp. \quad (5)$$

$\mathcal{H}_H$ has no off-diagonal matrix elements among the triplet states T_2x, T_2y, T_2z (or between these and the singlet or doublet); the states of the triplet therefore each give rise to a spin g tensor identical to that of the component valleys, i.e.,

$$\mathcal{H}_H(T_2x)=\beta[g_\parallel S_xH_x+g_\perp(S_yH_y+S_zH_z)], \quad (6)$$

etc. The g value for each triplet state is thus given simply by

$$g=(g_\parallel{}^2\cos^2\theta+g_\perp{}^2\sin^2\theta)^{1/2}, \quad (7)$$

where θ is the angle between $\mathbf{H}$ and the symmetry axis of the appropriate valleys. The doublet is more complicated, because $\mathcal{H}_H$ has both diagonal and off-diagonal matrix elements with respect to the degenerate states $E\theta$ and $E\epsilon$. We define two Hermitian operators $\mathfrak{U}_\theta$ and $\mathfrak{U}_\epsilon$ having matrix elements with respect to these states given by

$$\langle E\epsilon|\mathfrak{U}_\theta|E\epsilon\rangle=-\langle E\theta|\mathfrak{U}_\theta|E\theta\rangle=\langle E\theta|\mathfrak{U}_\epsilon|E\epsilon\rangle=+1;$$

thus, in this representation,

$$\mathfrak{U}_\theta=\begin{pmatrix}-1 & 0\\ 0 & +1\end{pmatrix},\quad \mathfrak{U}_\epsilon=\begin{pmatrix}0 & +1\\ +1 & 0\end{pmatrix}. \quad (8)$$

[17] Note that we label the irreducible representation of T_d to which the functions x, y, z belong (and also the functions yz, zx, xy) as T_2, whereas Kohn and Luttinger (Refs. 1 and 33) labeled this T_1. Our usage conforms to the original notation of Mulliken (Ref. 18) and to the widely accepted usage in the theory of transition metal ions [see, for example, J. S. Griffith, *The Theory of Transition Metal Ions* (Cambridge U. P., Cambridge, England, 1961) or C. J. Ballhausen, *Introduction to Ligand Field Theory* (McGraw-Hill, New York, 1962)]. Although most of the other work on shallow donor states in semiconductors (for examples, see Refs. 1 and 7) have continued to use Kohn and Luttinger's designation [which was in turn consistent with that of H. Eyring, J. E. Walter, and G. E. Kimball, *Quantum Chemistry* (Wiley, New York, 1944), p. 388], we believe it would minimize confusion if authors in this field would revert to the original Mulliken notation, as Castner (Ref. 50) has already done.

[18] R. E. Mulliken, Phys. Rev. **43**, 279 (1933).

[19] R. L. Aggarwal, Solid State Commun. **2**, 163 (1964); R. L. Aggarwal and A. K. Ramdas, Phys. Rev. **140**, A1246 (1965).

[20] H. Nara and A. Morita, J. Phys. Soc. Japan **23**, 831 (1967).

[21] L. M. Roth, Phys. Rev. **118**, 1534 (1960).

[22] H. Hasegawa, Phys. Rev. **118**, 1523 (1960).

The effect of $\mathcal{H}_H$ within the doublet state[23] may then be shown to be equivalent to that of

$$\mathcal{H}_H(E)=g_0\beta(\mathbf{S}\cdot\mathbf{H})-\tfrac{1}{6}(g_{\parallel}-g_{\perp})\beta\{[3S_zH_z-(\mathbf{S}\cdot\mathbf{H})]\mathfrak{U}_\theta +\sqrt{3}[S_xH_x-S_yH_y]\mathfrak{U}_\epsilon\}. \quad (9)$$

Taking $\hat{\zeta}$ to be a unit vector along $\mathbf{H}$ having components $\zeta_x, \zeta_y, \zeta_z$, and retaining only that portion of $\mathcal{H}_H(E)$ which is diagonal with respect to S_ζ, since $|g_{\parallel}-g_{\perp}|\ll g_0$, we have

$$\mathcal{H}_H(E)=g_0\beta S_\zeta H-\tfrac{1}{6}(g_{\parallel}-g_{\perp})\beta S_\zeta H \times[(3\zeta_z^2-1)\mathfrak{U}_\theta+\sqrt{3}(\zeta_x^2-\zeta_y^2)\mathfrak{U}_\epsilon]. \quad (10)$$

The resulting 2×2 secular equation for the eigenvalues of Eq. (10) is the same for both spin states $S_\zeta=\pm\frac{1}{2}$, except for an over-all sign change. The g values corresponding to the allowed spin transitions are given thus to first order in $(g_{\parallel}-g_{\perp})/g_0$ by

$$g=g_0\pm\tfrac{1}{3}(g_{\parallel}-g_{\perp})[1-3(\zeta_x^2\zeta_y^2+\zeta_y^2\zeta_z^2+\zeta_z^2\zeta_x^2)]^{1/2}. \quad (11)$$

The EPR spectrum of the doublet (in the absence of any splitting due to strain) is thus a pair of anisotropic lines which coincide (to first order in the small terms) for $\mathbf{H}$ in [111] and show the over-all cubic symmetry

C. Effect of Random Strain

The donor states are very sensitive to strain, the effect of which may be expressed[24,25] as

$$\mathcal{H}_S=\sum_{\alpha,\beta} e_{\alpha\beta}[\Xi_d\delta_{\alpha\beta}+\Xi_u\Sigma_j\mathcal{P}_j n_\alpha{}^j n_\beta{}^j]. \quad (12)$$

Here $e_{\alpha\beta}$ is a component of the strain tensor

$$e_{\alpha\beta}=\frac{1}{2}\left(\frac{\partial u_\alpha}{\partial x_\beta}+\frac{\partial u_\beta}{\partial x_\alpha}\right) \quad (13)$$

and Ξ_d, Ξ_u are the deformation potentials. Although simple dilatation displaces all the levels by the common amount $(\Xi_d+\frac{1}{3}\Xi_u)(e_{xx}+e_{yy}+e_{zz})$, and thus lifts no degeneracies, a strain giving rise to finite values for the components

$$e_\theta=e_{zz}-\tfrac{1}{2}(e_{xx}+e_{yy}),\qquad e_\epsilon=\tfrac{1}{2}\sqrt{3}(e_{xx}-e_{yy}) \quad (14)$$

lifts the fivefold degeneracy of the lithium ground state. The resulting energy displacements of the triplet states are given by

$$\Delta E(T_2x)=-\tfrac{1}{3}\Xi_u(e_\theta-\sqrt{3}e_\epsilon),\quad \Delta E(T_2y)=-\tfrac{1}{3}\Xi_u(e_\theta+\sqrt{3}e_\epsilon),\quad \Delta E(T_2z)=+\tfrac{2}{3}\Xi_u e_\theta. \quad (15)$$

As long as the strain splitting of the doublet is small compared with the valley-orbit splitting between the doublet and the singlet, the splitting of the doublet may be described by the equivalent operator

$$\mathcal{H}_S(E)=-\tfrac{1}{3}\Xi_u(\mathfrak{U}_\theta e_\theta+\mathfrak{U}_\epsilon e_\epsilon) \quad (16)$$

in terms of the matrices (8). The eigenstates of this operator are

$$|E+\rangle=\sin(\tfrac{1}{2}\psi)|E\theta\rangle+\cos(\tfrac{1}{2}\psi)|E\epsilon\rangle, \quad (17a)$$

$$|E-\rangle=\cos(\tfrac{1}{2}\psi)|E\theta\rangle-\sin(\tfrac{1}{2}\psi)|E\epsilon\rangle, \quad (17b)$$

corresponding to the energy displacements

$$\Delta E_\pm=\pm\tfrac{1}{3}|\Xi_u|(e_\theta^2+e_\epsilon^2)^{1/2}. \quad (18)$$

The angle ψ is defined by

$$\cos\psi=-(\Xi_u/|\Xi_u|)e_\theta(e_\theta^2+e_\epsilon^2)^{-1/2},\qquad \sin\psi=-(\Xi_u/|\Xi_u|)e_\epsilon(e_\theta^2+e_\epsilon^2)^{-1/2}. \quad (19)$$

With $\Xi_u\simeq11$ eV (see Sec. VII) and $(g_{\parallel}-g_{\perp})\sim10^{-3}$,[5] we see that even with strains $\sim10^{-8}$ the splitting of the E states given by Eq. (18) is larger than $(g_{\parallel}-g_{\perp})\beta H$. Internal strains are certainly this large, probably being more like 10^{-6}–10^{-5}. It is clear, therefore, that it is the internal random strains that determine the E-state wave functions at a particular lithium site, and not the anisotropy in the g factor, as considered in Sec. III B. We therefore take the diagonal matrix element of $\mathcal{H}_H(E)$ in Eq. (9) with respect to the states (17), obtaining

$$\langle\pm|\mathcal{H}_H(E)|\pm\rangle=g_0\beta(\mathbf{S}\cdot\mathbf{H})\mp\tfrac{1}{6}(g_{\parallel}-g_{\perp})\beta\{[3S_zH_z-(\mathbf{S}\cdot\mathbf{H})]\cos\psi +\sqrt{3}[S_xH_x-S_yH_y]\sin\psi\}. \quad (20)$$

We may define an angle α by

$$\cos\alpha=\tfrac{1}{2}(3\zeta_z^2-1)\times[1-3(\zeta_x^2\zeta_y^2+\zeta_y^2\zeta_z^2+\zeta_z^2\zeta_x^2)]^{-1/2}, \quad (21)$$

$$\sin\alpha=\tfrac{1}{2}\sqrt{3}(\zeta_x^2-\zeta_y^2)\times[1-3(\zeta_x^2\zeta_y^2+\zeta_y^2\zeta_z^2+\zeta_z^2\zeta_x^2)]^{-1/2}.$$

To first order in $(g_{\parallel}-g_{\perp})/g_0$, Eq. (20) then gives for the g factors of the strain-split doublet levels [for $(g_{\parallel}-g_{\perp})\beta H\ll(\Delta E_+-\Delta E_-)\ll$valley-orbit splitting] the result

$$g_\pm=g_0\mp\tfrac{1}{3}(g_{\parallel}-g_{\perp})[1-3(\zeta_x^2\zeta_y^2+\zeta_y^2\zeta_z^2+\zeta_z^2\zeta_x^2)]^{1/2}\times\cos(\psi-\alpha). \quad (22)$$

Finally, if the local strain at the site of different Li ions in the crystal is random in the absence of an externally applied stress, the angle ψ defined in Eq. (19) assumes at random any value in the range $(0,2\pi)$. The two

[23] The general form taken by the Zeeman interaction within the ^2E orbital doublet, as given by Eq. (9), is determined by symmetry considerations and is the same as that which has been used in studying a dynamic Jahn-Teller effect in the ^2E ground state of such transition metal ions in cubic symmetry as Sc^{2+} in CaF_2 and SrF_2 and Cu^{2+} in MgO [F. S. Ham, Phys. Rev. **166**, 307 (1968); see also Ref. 11]. The role of random strain in modifying the EPR spectrum of these Jahn-Teller ions is exactly the same as that described by the analysis leading to Eqs. (22) and (23).

[24] C. Herring and E. Vogt, Phys. Rev. **101**, 944 (1956).

[25] H. Brooks, in *Advances in Electronics and Electron Physics*, edited by L. Marton (Academic, New York, 1955), Vol. 7, p. 85.

resonance lines corresponding to Eq. (22) are accordingly broadened. It is straightforward to show that the shape function of the resulting line is given by

$$f(g)dg=\frac{(1/\pi)dg}{[(\Delta g)^2-(g-g_0)^2]^{1/2}} \tag{23}$$

for $(g_0-|\Delta g|)<g<(g_0+|\Delta g|)$ and $f(g)=0$ for $|g-g_0|>|\Delta g|$. This strain-broadened line is shown by the curve labeled $K^{-1}\Delta g=\infty$ in Fig. 3(a). The edges of the line are therefore sharp, and they coincide with the positions of the lines expected from Eq. (11) for the doublet spectrum for zero strain.

D. Relaxation Effects in Doublet Spectrum

Because of the strong strain coupling among the doublet states as described by Eq. (16) and between the E and A_1 states as found from Eq. (12), these states can be expected to be strongly coupled to the lattice phonons. The lifetime of the two E eigenstates may therefore be short as a result of phonon-induced transitions between them. The effect of this relaxation upon the strain-broadened shape function (23) can be estimated as follows.

At any particular lithium site, the states $|E+\rangle$ and $|E-\rangle$, which are eigenstates in the local strain, give rise to resonances at $g_0+\delta g$ and $g_0-\delta g$, according to Eq. (22). The resonance angular frequencies for these states are therefore at $(g_0\pm\delta g)\beta H/\hbar$. The line shape resulting from a relaxation between two discrete resonance frequencies has been worked out previously for the effect of chemical exchange or motional hopping in NMR studies.[26] The result, expressed as a normalized shape function for the distribution in g corresponding to a fixed value of δg, is

$$I(g,\delta g)=\frac{(1/\pi)(\delta g)^2K}{[(g-g_0)^2-(\delta g)^2]^2+(g-g_0)^2K^2} \tag{24}$$

for the case in which there is equal probability of finding the system in either state. Here we define

$$K^{-1}=\tfrac{1}{2}\tau\beta H/\hbar, \tag{25}$$

where τ is the average lifetime of each state.

Averaging over the distribution in δg resulting from the random strains, we obtain from Eq. (24) the line-shape function

$$F(g)=\int_{-\Delta g}^{+\Delta g} f(g_0+\delta g)I(g,\delta g)\,d(\delta g), \tag{26}$$

where $f(g_0+\delta g)$ is given by Eq. (23). We have calculated $F(g)$ for several values of $K^{-1}\Delta g$; the results are shown in Fig. 3(a).

We see from Fig. 3(a) that when the relaxation time is long ($K^{-1}\Delta g\gg1$), the line shape of the doublet spectrum approaches that of the strain-broadened distribution, and we expect to see the sharp edges, as discussed in Sec. III C. When the relaxation time is short ($K^{-1}\Delta g\ll1$), we see only a single line at the center of gravity of the strain-broadened distribution. At intermediate relaxation times ($K^{-1}\Delta g\sim1$–10), one has existing simultaneously both a line at the center and peaks at the edges of the broadened line.

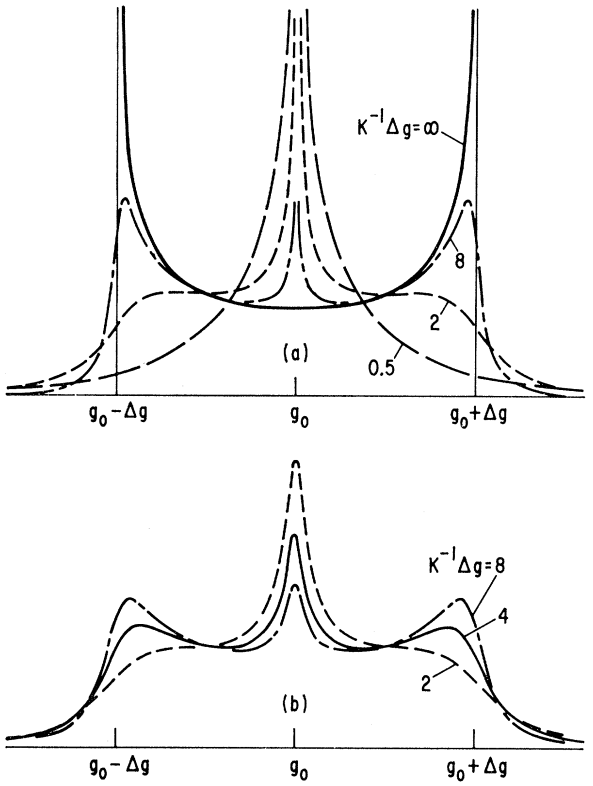

FIG. 3. Strain-broadened EPR line shape predicted for the doublet E states and the effect of phonon-induced relaxation within the doublet: (a) no additional source of broadening, (b) a weak additional Lorentz broadening (with T_2 taken to be equal to $20\hbar/\beta H\Delta g$). K is related to the average lifetime τ of each state by Eq. (25) in the text.

The curves of Fig. 3(a) do not include the effects of broadening sources other than strain. These will have the effect of smoothing out the curves and removing the divergences. For example, Fig. 3(b) shows the effect on the final line shape for the analytically convenient case in which the additional sources produce a Lorentzian line shape for the individual resonance lines. These curves were calculated in the same manner as those of Fig. 3(a), but with Eq. (24) replaced by the more general expression including the small Lorentz broadening.[27] Although the Lorentz broadening is not necessarily realistic, the curves of Fig. 3(b) serve as a reasonable guide to the shapes to be expected. They demonstrate clearly that in the transition region three well-

[26] H. S. Gutowsky and A. Saika, J. Chem. Phys. **21**, 1688 (1953).

[27] Derived directly from Eq. (18) of Ref. 26.

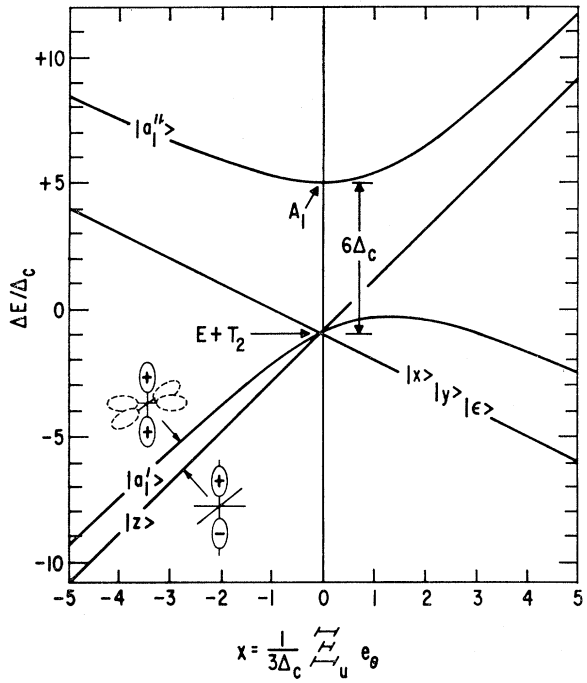

FIG. 4. Energy levels of the 1s hydrogenic states of the lithium donor as a function of applied tetragonal strain e_θ (after R. L. Aggarwal, P. Fisher, V. Mourzine, and A. K. Ramdas, Ref. 7, Fig. 15).

resolved peaks due to the doublet spectrum can exist simultaneously.

E. Effect of Applied Uniaxial Stress

When the strain splitting is not small compared to the valley-orbit splitting, the interaction of the doublet with the singlet must be taken into account. In particular, for an applied uniaxial stress T along the [001] direction we have

$$\begin{aligned} e_\theta &= (S_{11}-S_{12})T_{[001]}, \\ e_\epsilon &= 0, \end{aligned} \tag{27}$$

where S_{11} and S_{12} are the appropriate elastic compliance moduli. Alternatively, for stress applied along the [110] direction,

$$\begin{aligned} e_\theta &= -\tfrac{1}{2}(S_{11}-S_{12})T_{[110]}, \\ e_\epsilon &= 0. \end{aligned} \tag{28}$$

Defining

$$x=\tfrac{1}{3}(\Xi_u/\Delta_c)e_\theta, \tag{29}$$

where $6\Delta_c$ denotes the energy of the singlet relative to that of the doublet,[28] we find that the (relative) displacements of the triplet states and of the doublet state $E\epsilon$ for either stress are then given from Eqs. (15) and (16) to be

$$\begin{aligned} &\Delta E(E\epsilon)=\Delta E(T_2x)=\Delta E(T_2y)=-x\Delta_c, \\ &\Delta E(T_2z)=+2x\Delta_c. \end{aligned} \tag{30}$$

The energies of the states derived from the doublet state $E\theta$ and the singlet state A_1 are given[5,7] relative to the energy of the doublet in zero strain by

$$E=\Delta_c[3+\tfrac{1}{2}x\pm\tfrac{1}{2}(36-12x+9x^2)^{1/2}]. \tag{31}$$

These energy levels are plotted as a function of the strain in Fig. 4. The common shift of all the levels due to dilatation is omitted from Eqs. (30) and (31) and from Fig. 4. The g factor of the lower-energy state in Eq. (31) is found (after Wilson and Feher[5]) to be given from Eq. (4) to first order in $(g_{11}-g_1)/g_0$ by

$$\begin{aligned} g=g_0+\tfrac{1}{6}(g_{11}-g_1)(1-\tfrac{3}{2}\sin^2\theta) \\ \times[1-3(3x-2)(36-12x+9x^2)^{-1/2}], \end{aligned} \tag{32}$$

where θ here is the angle between $\mathbf{H}$ and the [001] axis.[29]

F. Summary

From the conclusion of Aggarwal *et al.*[7] that the Li ground state is fivefold degenerate or very nearly so, comprising the doublet and triplet levels, we would expect that the Li EPR spectrum for zero applied stress should be the superposition of the spectra of these five states, at least at temperatures low enough to eliminate relaxation effects. For the independent-valley model considered so far, the triplet state should not be affected by random strains and should contribute three lines with g factors given by Eq. (7). Random strains do affect the doublet, however. In the absence of relaxation effects, the strains should cause the doublet to give rise to the powder-pattern type of line described by Eqs. (22) and (23), with peaks at the positions given by Eq. (11). Relaxation between the doublet states will tend to average out the powder-pattern line shape, the exact shape depending upon the relaxation time as indicated in Fig. 3.

IV. GENERAL EXPERIMENTAL RESULTS AND DISCUSSION

A. Zero-Stress Spectrum

The spectrum in an unstressed crystal at ~20 kMc/sec is shown in Fig. 5(a). Because of the breadth of the spectrum, it appears weak and is easy to overlook. However, the *integrated* intensity is sizable, correlating closely with the electrically measured lithium content

[28] It is convenient to consider the energy parameter Δ_c to be *positive*, and we shall follow this practice throughout this paper.

[29] An expression for the components of the g tensor for Li in Si under uniaxial compression has been obtained also by T. Shimizu [J. Phys. Soc. Japan **20**, 1096 (1965)]. His result is equivalent to our Eq. (32) if an error in his Eq. (2) is corrected, where the coefficient of g_l-g_t should be $+\frac{1}{4}$ instead of $+\frac{1}{2}$; note that the parameter x used by Shimizu is the *negative* of our x as defined in Eq. (29).

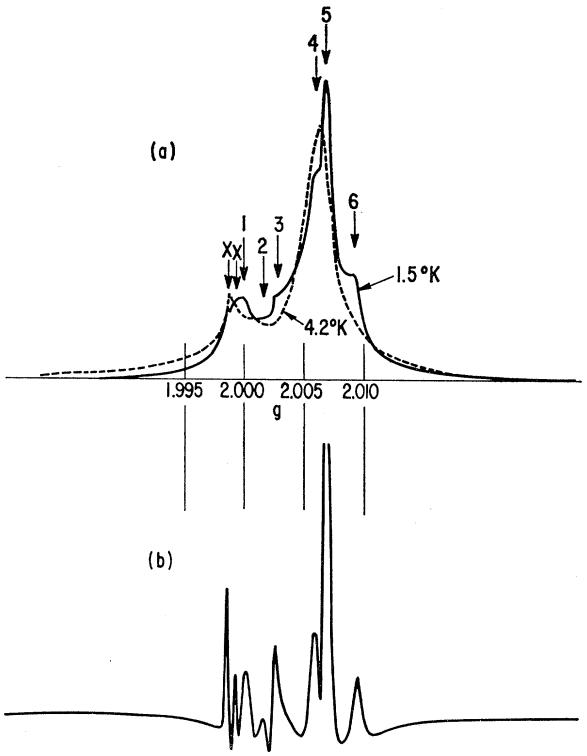

FIG. 5. EPR spectrum in lithium-doped ($\sim 10^{16}$-cm^{-3}) vacuum floating-zone silicon at zero applied stress, $\mathbf{H} \| \langle 100 \rangle$, $\nu_0 \simeq 20$ kMc/sec: (a) absorption at 4.2 and 1.5°K, (b) derivative of dispersion at 1.5°K.

in the samples.[30] There is little change in the character of the spectrum between ~ 2.5 and 20°K, being broad with evidence of only partially resolved anisotropy. Below ~ 2.5°K additional structure emerges as shown in the figure. Careful study of the intensity of the spectrum through the range 1.5–4.2°K revealed that the integrated intensity, corrected for the $1/T$ Boltzmann dependence, is roughly constant.

As seen in Fig. 5, this structure is only partially resolved. Some gain in resolution is achieved by recording the derivative of dispersion using normal magnetic field modulation as shown in Fig. 5(b). The deduced angular dependence of the spectrum at 1.5°K and 20 kMc/sec is shown in Figs. 6(a) and 6(b).[31] It is apparent that considerable complexity is present. The curves are drawn only where the connection of the observed points is obvious. The poor resolution of these overlapping lines does not allow an unambiguous connection of points throughout. No apparent difference in the spectrum was observed between a Li^6- and Li^7-doped sample.

The spectrum has also been studied at 9.4 and 14 kMc/sec. These results are plotted in Fig. 7, along with those at 20 kMc/sec, and they reveal that the apparent g values of the spectral lines vary *linearly* with H^{-2} (or

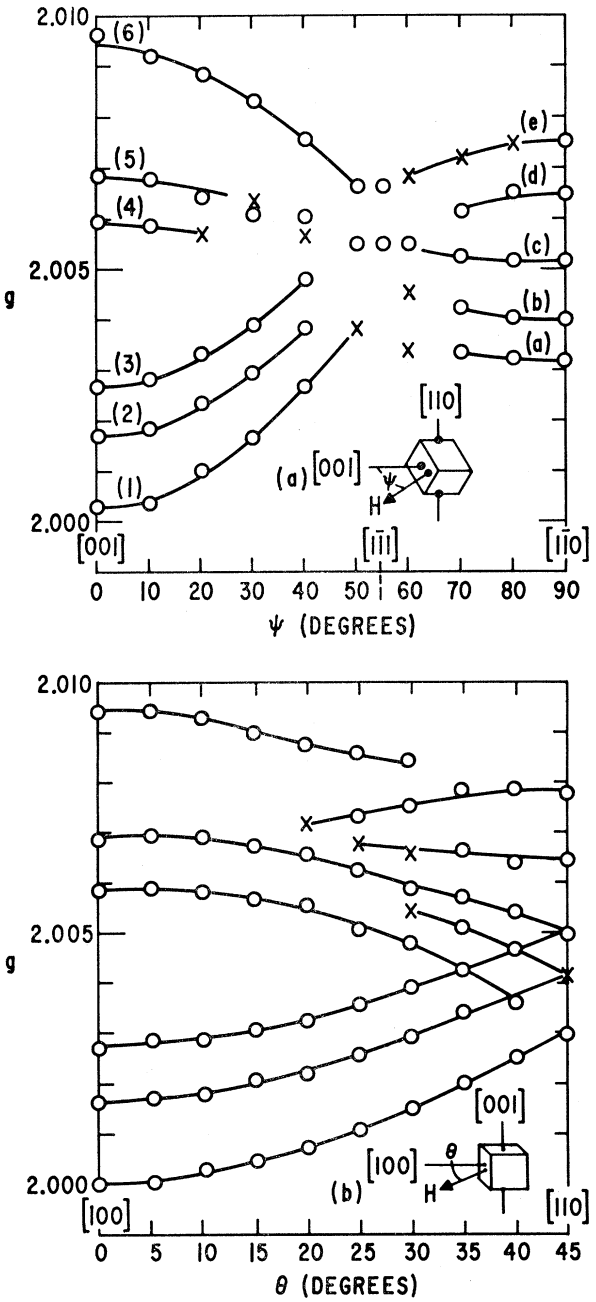

FIG. 6. Angular dependence of the lithium donor EPR spectrum at 1.5°K, $\nu_0 \simeq 20$ kMc/sec, zero applied stress: (a) **H** in the (110) plane; (b) **H** in the (001) plane.

[30] The calibration for this measurement was made by comparison with the integrated absorption of the shallow donor spectrum of phosphorous-doped silicon of known phosphorous concentration.

[31] The set of lines in Fig. 5 labeled "x" have not been included in Fig. 6. They arise from a $\langle 100 \rangle$ distorted center with $g_{\parallel} = 1.9993 \pm 0.0003$, $g_{\perp} = 1.9987 \pm 0.0003$. This center was present with varying intensity in all samples studied but was always very much weaker than the remainder of the spectrum. This is presumably the same center recently studied by F. E. Geiger [NASA Technical Report No. NASA TR-R-290 (unpublished)] and may arise from a lithium donor paired with some other defect. It is not, however, the same center identified by Feher (Ref. 3) as the Li-O donor which has $\langle 111 \rangle$ symmetry. We will not concern ourselves further in this paper with this center.

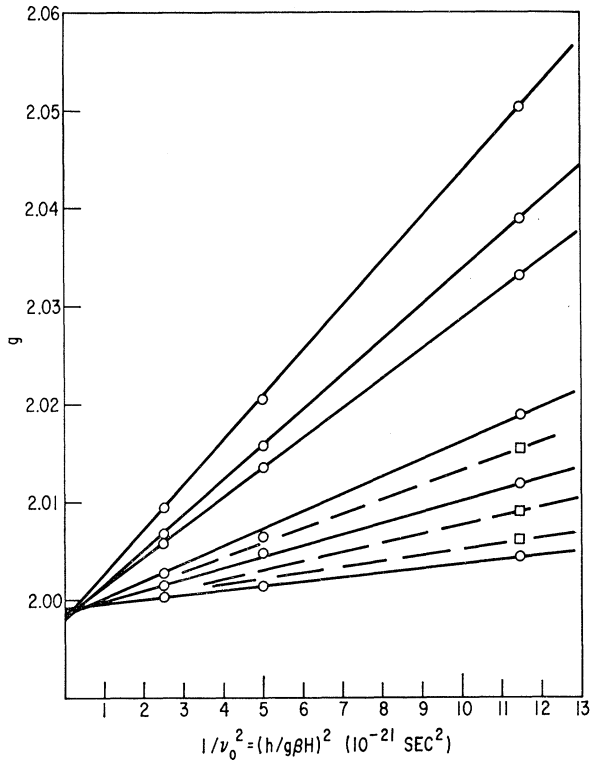

FIG. 7. Dependence of the apparent g value of the lithium donor EPR spectrum at 1.5°K on microwave frequency. The solid lines denote the zero stress values for H‖[001]. The dashed lines are for large [110] compression, H‖[001].

ν_0^{-2}). Extrapolated to infinite magnetic field, the g values range between $\sim$1.998 and $\sim$1.999.

B. Spectrum with Stress

The spectrum changes markedly upon the application of uniaxial stress. This is seen in Fig. 8 for the application of compressional stress along the [001] direction. The initial effect is seen to be a broadening and shifting of the spectrum toward higher g values. Upon higher stress, broad lines begin to emerge from *lower* g values, sharpening up and, in the case of Fig. 8, ending up in a single sharp intense line at $g=1.9987$. The effects of compression and tension along both the [001] and [110] directions are summarized graphically in Figs. 9 and 10. In each of these cases, the total integrated intensity appears constant throughout the transformations versus stress.

For both [001] compression and [110] tension, a single sharp intense line emerges at high stresses. This line is described by an axially symmetric g tensor independent of magnetic field, with[32]

$$g_{\parallel}=1.9997\pm0.0001, \quad g_{\perp}=1.9987\pm0.0001.$$

[32] These values were estimated by comparison to the shallow donor resonance of phosphorus at $g=1.9985\pm0.0001$ (Ref. 3) in a small sample of phosphorus-doped silicon ($\sim3\times10^{16}$/cm^3) glued to the side of the lithium-doped sample.

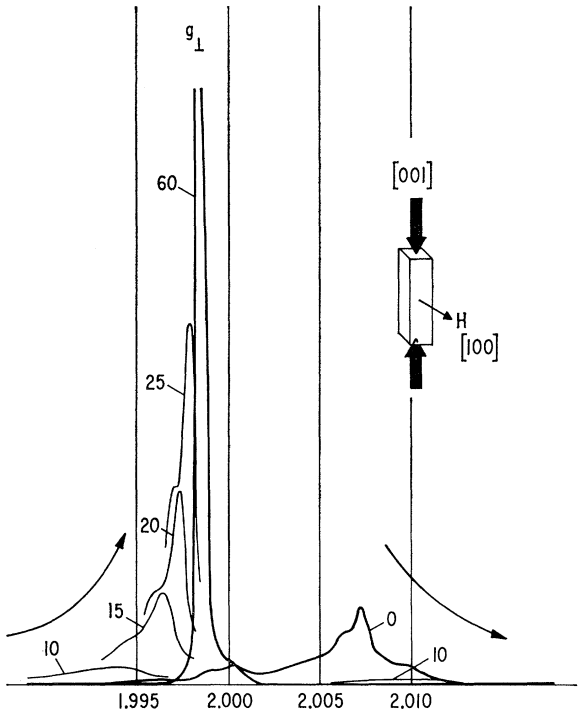

FIG. 8. Lithium donor EPR spectrum as a function of [001] compressional stress (indicated values in kg/cm^2), with H‖[100], $\nu_0\simeq20$ kMc/sec, $T=1.5$°K.

For the [001] compression, $g_{\parallel}$ is along the stress direction. For [110] tension, $g_{\parallel}$ is along the [001] direction (which lies in the plane perpendicular to the stress direction). The angular dependence of the line in the (110) plane for [110] tension is shown in Fig. 11(a). The

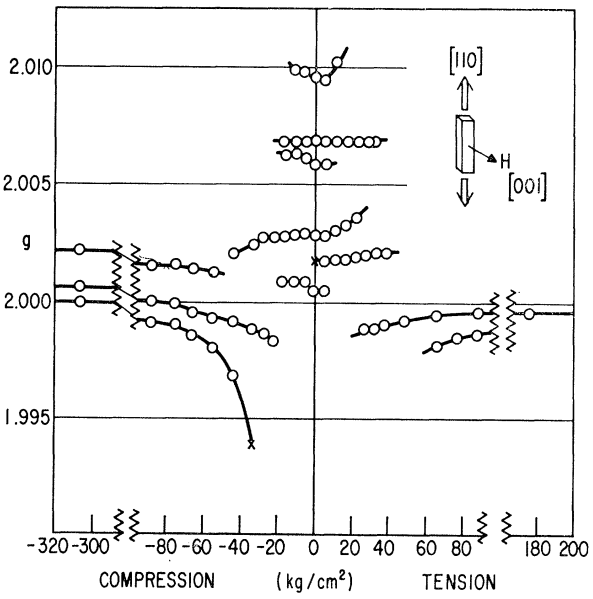

FIG. 9. Spectrum g values versus [001] applied stress, H‖[100], $\nu_0\simeq20$ kMc/sec, $T=1.5$°K.

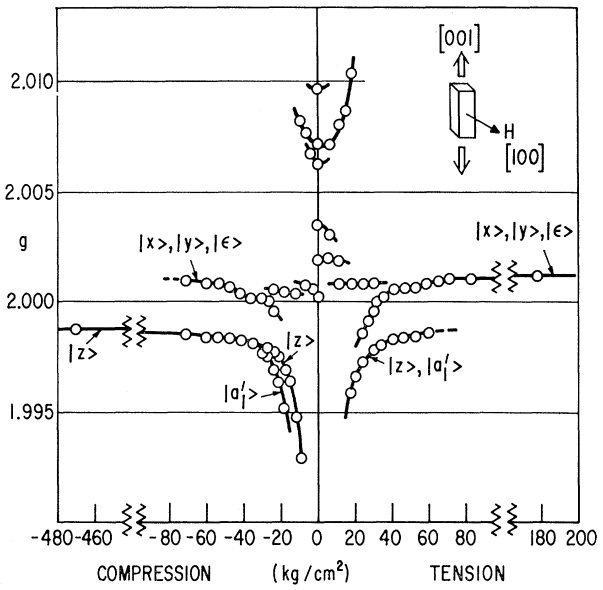

FIG. 10. Spectrum g values versus [110] applied stress, $\mathbf{H}\|[001]$, $\nu_0\simeq 20$ kMc/sec, $T=1.5°$K.

shape of the line is roughly Gaussian with a full width at half-maximum (FWHM) of 1.3 G.

In the high-stress limit for [001] tension or [110] compression, the spectrum has also simplified and the lines sharpened, but not so much as for the reverse stresses. The angular dependence in the (110) plane for [110] compression is given in Fig. 11(b). Again, as shown in Fig. 7, the g values vary linearly with H^{-2}.

C. Discussion

These results appear to confirm the general picture deduced by Aggarwal *et al.*[7] The complexity of the zero-stress spectrum and its extreme sensitivity to externally applied stress confirm the degeneracy (or near-degeneracy) of the ground state. In addition, [001] compression or [110] tension, which should remove this degeneracy as in Fig. 4, greatly simplifies the spectrum, as expected.

In the case of [001] compression or [110] tension, the ground state is expected to be the T_2z state, which is simply the antisymmetric pair of [001] valleys. Consistent with this, a single axially symmetric spectrum is observed whose g tensor is oriented along the z cube axis. The observed anisotropy $(g_{\parallel}-g_{\perp})$ of $+1.0\pm0.1\times10^{-3}$ is in close agreement with that estimated by Wilson and Feher[5] $[(+1.04\pm0.04)\times10^{-3}]$ for a single valley from stress experiments on the phosphorus donor resonance. Their results, combined with the free-conduction electron-resonance g value of 1.99875 ± 0.00010,[3] predict for a single conducting-band valley

$$g_{\parallel}=1.9994\pm0.0001, \quad g_{\perp}=1.9984\pm0.0001.$$

The values observed for the lithium donor are slightly higher ($+0.0003$) than these, and this difference is outside the combined estimate of errors. However, shifts of comparable magnitude (but of opposite sign) are also observed for the substitutional donors. Shifts of this magnitude, presumably originating from small central-cell effects, should therefore not be considered unreasonable.

The simple theory outlined in Sec. III therefore appears to adequately describe the spectrum when applied uniaxial stress has removed the degeneracy of the ground state. It is apparent, however, that it is not adequate to describe the spectrum when degeneracy remains. For zero stress, the theory predicted a complex spectrum, but with all components confined to the narrow range between the values of $g_{\parallel}$ and $g_{\perp}$ for a single valley. Instead, the observed spectrum spreads over a larger range of g values, all higher than $g_{\parallel}$ or $g_{\perp}$. Similar departures are also observed for [001] tension and [110] compression, where the degeneracy is only partially removed. In addition, the theory does not account for the H^{-2} dependence of the g values (Fig. 7) nor for the dramatic effects of stress in the low-stress transition region (Figs. 9 and 10).

The failure of the simple theory when degeneracy remains suggests the importance of some interaction involving matrix elements between the states, which was not included in the treatment of Sec. III. This interaction is apparently small because modest stress splittings are sufficient to quench its effect, as is evidenced by the success of the simple theory under [001] compression and [110] tension. On the other hand, it is clear that it must be included when degeneracy remains in the

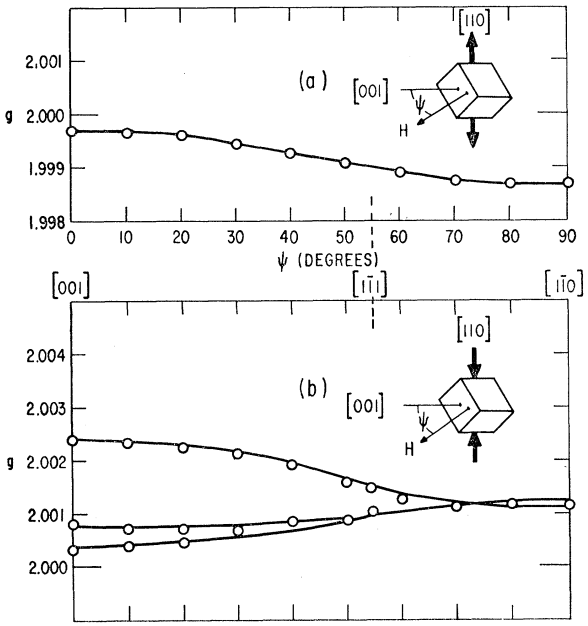

FIG. 11. Angular dependence of the EPR spectrum under large [110] stress, $\nu_0\simeq 20$ kMc/sec, $T=1.5°$K: (a) 175-kg/cm² tension; (b) 480-kg/cm² compression.

ground state. We will return to this in Sec. VI. First, however, we will examine in more detail the spectrum under high [001] compression or [110] tension where the theory of Sec. III is applicable.

V. SPECTRUM UNDER [001] COMPRESSION OR [110] TENSION

A. Linewidth

The linewidth of 1.3 G (FWHM) is considerably narrower than that measured for the nonstressed shallow-donor resonance of substitutional phosphorus, 2.5 G.[3] As pointed out by Kohn[1] and Feher,[3] the origin of these widths is the inhomogeneous broadening due to hyperfine interactions with Si^{29} nuclei within the electron orbit. Let us therefore make an estimate of the expected linewidth to see if this large difference is reasonable.

Following Kohn,[1] we estimate the second moment of the line by

$$\langle \Delta H^2 \rangle = (0.047) \sum_l (\Delta H_l)^2 . \tag{33}$$

Here,

$$\Delta H_l = + (8\pi/3)(\mu^{29}/I) |\Psi(\mathbf{r}_l)|^2 m_l \tag{34}$$

is the local field seen by the electron due to the Fermi contact interaction with a Si^{29} nucleus with magnetic quantum number m_l, moment μ^{29}, and spin $I = \frac{1}{2}$, at the lth site. In summing over all sites in (33), we have included the factor 0.047 for the isotopic abundance of Si^{29}. For $\Psi(\mathbf{r})$ we take the Kohn-Luttinger wave function given by Eqs. (1)–(3) with $F_j(\mathbf{r})$ for the valleys at $[0, 0, \pm k_0]$ given by

$$F_z(\mathbf{r}) = (\pi n^3 a^2 b)^{-1/2} \exp\left\{ -\left[\frac{(x^2+y^2)}{n^2 a^2} + \frac{z^2}{n^2 b^2} \right]^{1/2} \right\} , \tag{35}$$

where n is taken to be the square root of the ratio of the effective-mass binding energy[1,33] (29 meV)[34] to the actual Li binding energy[7] (33 meV),

$$n = 0.937 . \tag{36}$$

This form for $F_j(\mathbf{r})$ represents a simple correction[3] to the effective-mass variational solution[33] to account for the fact that the observed binding energy departs from the effective-mass value. Better approximations[33] could perhaps be used but would be less convenient to handle; since n for lithium is very close to unity, such improvements should not be large. In (35), a and b are the effective Bohr radii in the perpendicular and parallel directions that result from the variational solution of the effective-mass bound-donor equation. They have the values[1] $a = 25.0 \times 10^{-8}$ cm, $b = 14.2 \times 10^{-8}$ cm.

For high [001] compression or [110] tension, we expect from Fig. 4 that the lithium-donor wave function in the lowest-energy state will be the antisymmetric combination of the two z valleys, so that from Eqs. (1)–(3) and (35) we have for this state at the lth lattice site

$$\Psi(\mathbf{r}_l) = i F_z(\mathbf{r}) u_z(\mathbf{r}_l) \sqrt{2} \sin k_0 z , \tag{37}$$

the origin of coordinates being the site of the lithium ion. The square of the wave function at the lth site is therefore

$$|\Psi(\mathbf{r}_l)|^2 = 2\eta F_z^2(\mathbf{r}) \sin^2 k_0 z , \tag{38}$$

where

$$\eta = |u_z(\mathbf{r}_l)|^2 / \langle |u_z(\mathbf{r})|^2 \rangle , \tag{39}$$

the average being taken over the unit cell. For η we take the value 178 obtained from nuclear relaxation time measurements by Shulman and Wyluda[35] (as corrected by Wilson and Solomon[36]), and for k_0 the value[3] $k_0 = 0.085 k_{\max}$. With the lithium ion at a tetrahedral interstitial site, the silicon lattice sites fall on the planes $z = m(a_0/4)$ with $m = 0, \pm 1, \pm 2, \ldots$. In the evaluation of Eq. (33), we have determined the contribution from each plane with z constant by replacing the summation over the sites within the plane by an integral,[37] and we have then carried out the summation over these planes. The result $(\Delta H^2)^{1/2} = 0.58$ G corresponds to a calculated value for the FWHM $\Delta H_{1/2} = 1.37$ G [assuming a Gaussian line shape, for which $\Delta H_{1/2} = (2.36)(\Delta H^2)^{1/2}$]. This result is in good agreement with the observed value of 1.3 G.

We have also evaluated $(\Delta H^2)^{1/2}$ for the symmetric combination of the two z valleys, using $\cos k_0 z$ in place of $\sin k_0 z$ in Eqs. (37) and (38). This calculation also yielded $(\Delta H^2)^{1/2} = 0.58$ G, the small difference ($\simeq 0.1\%$) actually obtained between the results for the symmetric and antisymmetric combinations being much less than our estimate of the error involved in replacing the summation within the planes by integration. The experimental linewidth thus does not enable one to confirm that the antisymmetric combination of the valleys is actually the lower-energy state in the stressed crystal. Moreover, these values for $(\Delta H^2)^{1/2}$ agree to within the estimated error with what one obtains by replacing $\sin^4 k_0 z$ or $\cos^4 k_0 z$ by their average value ($\frac{3}{8}$). The line-

[33] W. Kohn and J. M. Luttinger, Phys. Rev. **97**, 883 (1955); **98**, 915 (1955).

[34] In a paper that appeared after the work reported here was completed, R. A. Faulkner [Phys. Rev. **184**, 713 (1969)] has suggested that the value for the low-temperature dielectric constant appropriate to the effective-mass calculation of the donor levels in silicon should be taken to be $\kappa = 11.40 \pm 0.05$, and he has shown that the corresponding value of the effective-mass binding energy is 31 meV. The calculations in the present paper were all done assuming the Kohn-Luttinger values for the binding energy (29 meV) and the effective Bohr radii a and b. Substitution of the improved values would make only a small change in our quantitative results.

[35] R. G. Shulman and B. J. Wyluda, Phys. Rev. **103**, 1127 (1956).

[36] D. K. Wilson, Phys. Rev. **134**, A265 (1964). See Ref. 31.

[37] Comparison of the result obtained by actual summation in the plane $z = 0$ with the value of the corresponding integral (for the case of the symmetric pair of valleys) indicated that the error in $\Delta H_{1/2}$ caused by the use of integration instead of summation is less than 2%.

width in this case thus appears to be insensitive to the value of k_0.[38]

The result that the line is much narrower for the lithium donor in stressed silicon than for the phosphorus donor (in the absence of stress) has its origin in two separate effects. The first is that the lithium donor is shallower (33 as opposed to 44 meV), and therefore more spread out. From the preceding formulas one can show that $(\Delta H^2)^{1/2}$ scales roughly as $n^{-3/2}$, so that this effect by itself would cause the lithium resonance to have a width $\sim 80\%$ that of the phosphorus. The second source of the difference is that the lithium wave function involves only two valleys and is therefore oscillatory in only one direction, while for the phosphorus the wave function is the symmetric combination of all six valleys, which is oscillatory in all directions through the factor $[F_x \cos k_0 x + F_y \cos k_0 y + F_z \cos k_0 z]$. Taking the appropriate normalization factors into account from Eq. (3) and replacing the factors $\sin^4 k_0 z$, $\cos^4 k_0 z$, $\cos^2 k_0 x$, $\cos^2 k_0 y$, etc., by their average values as above, we find that this difference in the oscillatory behavior introduces into the ratio $(\Delta H^2)_{\mathrm{Li}}{}^{1/2}/(\Delta H^2)_{\mathrm{P}}{}^{1/2}$ a further factor given approximately by $\xi = \sqrt{3}/(1+4u)^{1/2}$, where $u = \langle F_x{}^2 F_y{}^2 \rangle_{\mathrm{av}} / \langle F_z{}^4 \rangle_{\mathrm{av}}$. Using for u the estimate 0.86, we obtain for ξ the value 0.82. Both effects on the linewidth ratio thus appear to contribute more or less equally.

B. ENDOR

1. Experimental Results

For most conditions of stress, temperature, etc., the lithium resonance lines were well relaxed, and no saturation of the absorption lines was observed. This was not true, however, for the single line observed under [001] compression or [110] tension. This line was easily saturated at $\lesssim 4$°K for stresses $\gtrsim 100$ kg/cm^2, making ENDOR studies possible. Most of the ENDOR studies on this line were performed for [001] compressional stress, and both Li^7 (or Li^6) and Si^{29} transitions were observed. The lithium transitions showed no anisotropy versus magnetic field orientation in the plane perpendicular to the stress. The Si^{29} transitions were weaker and their angular dependence was not studied in detail. A cursory study indicated that anisotropies may exist for some of the lines in the plane, but that they are small.

The ENDOR transitions were described by

$$h\nu_j = |MA_j - (\mu_j/I_j)H| , \qquad (40)$$

the relation appropriate for an isotropic hyperfine constant A_j and no quadrupole interaction. Both the $M = +\frac{1}{2}$ and $M = -\frac{1}{2}$ transitions were studied for the lithium. For Si^{29} only the frequencies above $\mu H/Ih$ were studied.

In Fig. 12 the values of A_j for the resolved Si^{29} ENDOR transitions and for Li^7 under 470-kg/cm^2 compressional [001] stress are shown as a function of temperature for H parallel to [100]. The Li hyperfine interaction is observed to increase by an order of magnitude as the temperature is raised from 1.3 to 4.2°K. In a sample doped with Li^6, the same variation was observed, and, within the accuracy of measurement, the ratio of the hyperfine constants at any temperature was given by the ratio of the nuclear gyromagnetic ratios of Li^6 and Li^7. The resolved Si^{29} hyperfine interactions also vary slightly with temperature, in this case decreasing with increasing temperature.

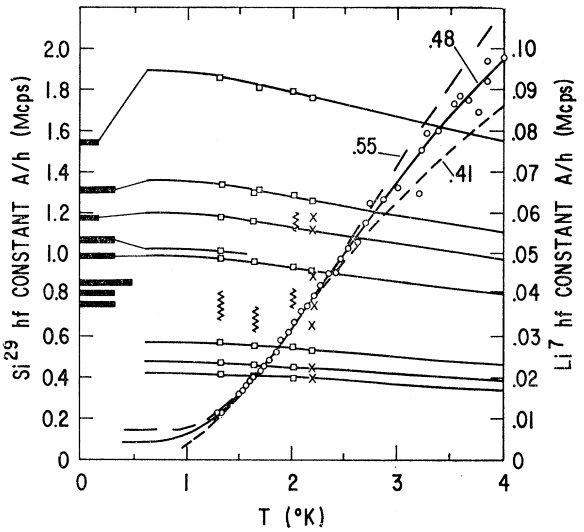

FIG. 12. Temperature dependence of the Li^7 and the resolved Si^{29} hyperfine interactions as determined by ENDOR under 470-kg/cm^2 [001] compressional stress, $\mathbf{H} \| [100]$. The curves are theoretically derived for different assumed values of the energy separation (indicated in meV) between the z and a_1' states and with $\Xi_u = 11.4$ eV. The bars on the left indicate the positions and relative amplitudes predicted for the neighboring Si^{29} interactions by the simple effective-mass treatment outlined in the text.

At a given temperature, the lithium hyperfine constant also varies somewhat with the magnitude of the stress, as shown in Fig. 13. The possible effect of additional off-axis shear stress on the lithium hyperfine splitting was also studied. For this purpose, crystals were cut with the stress axis at 17° and 35° with respect to the [001] axis in the (110) plane. In each sample, sharp Li^7 ENDOR transitions were observed with the splitting given solely by the net excess stress component resolved along the [001] direction [i.e., the resolved component of e_θ, Eq. (14)]. Similar results were obtained for a crystal oriented 15° from the [001] axis in the (100) plane. We conclude, therefore, that the hyperfine splitting is determined solely by the resolved compressional stresses along the cube directions and is not affected by the off-axis shear strains e_{yz}, e_{zx}, and e_{xy}.

2. Discussion

From the relation

$$A_l = (16\pi/3)(\mu_l/I_l)\beta |\Psi(\mathbf{r}_l)|^2 \qquad (41)$$

[38] This conclusion contrasts with that of Kohn (Ref. 1) for the singlet ground state of the substitutional donors. There the dependence on k_0 was found to be sufficiently great to enable Kohn to make a rough estimate of k_0 from the observed linewidth.

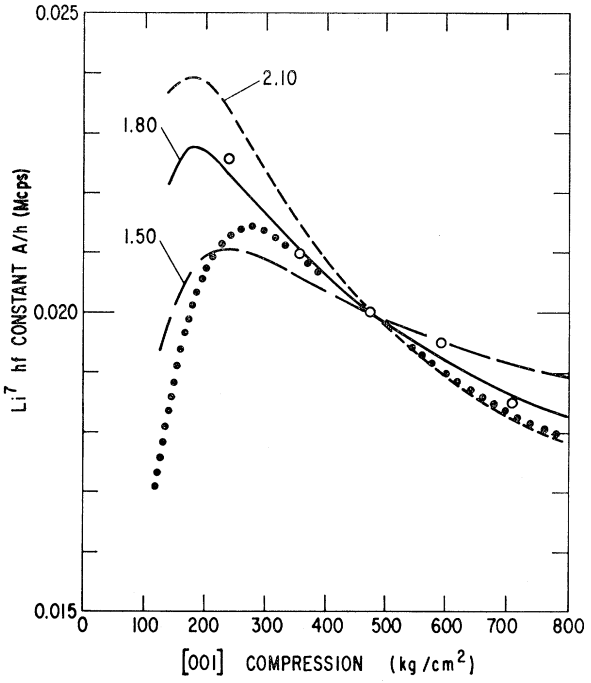

FIG. 13. Stress dependence of the Li^7 hyperfine interaction at $T=1.66°K$. The solid and dashed curves are theoretically derived for different assumed values of the valley-orbit splitting ($6\Delta_c$, indicated in meV), and with $\Xi_u=11.4$ eV. The dotted curve is for $6\Delta_c=1.8$ meV and $\Xi_u=7.9$ eV.

for the isotropic part of the hyperfine interaction at the lth atom site, and using Eqs. (35) and (38) to obtain $|\Psi(\mathbf{r}_l)|^2$ for the antisymmetric combination of the two z valleys, we can calculate the Si^{29} hyperfine interactions predicted by this model. The relative importance of the silicon atoms lying in the different planes $z=m(\frac{1}{4}a_0)$ is indicated if we set $x=y=0$ in Eqs. (35) and (38) and consider the z dependence of $\sin^2 k_0 z \exp(-2|z|/nb)$, which has the values 0, 0.771, 0.137, 0.314, 0.289, 0.053, 0.287, 0.001, 0.177, respectively, in the planes with $|m|=0, 1, 2, 3, \ldots$ for $k_0=0.85(2\pi/a_0)$. The value for the planes with $m=\pm 1$ is more than twice as large as that for any other plane, and we see, therefore, that the larger hyperfine splittings arise from the silicon atoms in this first pair of planes. The results for the nearest 30 atoms in each of these two planes are indicated on the ordinate in Fig. 12 ,where the amplitude of each bar is proportional to the number of equivalent atom sites giving each value. We have ignored anisotropies in the interaction. With the exception of the nearest atom site, for which the wave function is expected to be the poorest, there appears to be a rough one-to-one correlation for the larger resolved splittings. The resolved transitions at $A/h=0.57$ Mc/sec and lower may represent the contributions from other planes. The larger experimental value for the nearest atom site (occupied by the four nearest-neighbor atoms to the lithium) presumably reflects an enhanced concentration of the wave function, near the lithium ion, over that predicted by Eq. (35).

In this model, there is a node for the T_2z wave function in the $z=0$ plane, and the hyperfine interaction with the lithium should be very close to 0. The values, as shown in Fig. 12, are indeed small. By way of comparison, Feher[3] reported the value 845 kc/sec for the Li^7-oxygen complex donor. At low temperatures, the data of Fig. 12 extrapolate to near 0, and we conclude therefore that the identification of the ground state under [001] compression or [110] tension as the T_2z antisymmetric pair of valleys is confirmed.

Let us consider the temperature dependence of the Li^7 interaction shown in Fig. 12. Three possible explanations suggest themselves, two of which we can rule out immediately. First, we might suppose that lattice phonons directly alter the T_2z ground-state wave function by admixing excited states, presumably the nearby state labeled a_1' in Fig. 4, which is derived from the states A_1 and $E\theta$ in accord with Eq. (31) and which represents the symmetric combination of the z valleys in the limit of large stress. Because the temperature dependence of Fig. 12 is almost linear in T, this explanation would require that the relevant phonons be in the classical regime at these temperatures, or in other words that they have energies $(\hbar\omega/k)\lesssim T\sim 2°K$. Such phonons of the silicon lattice would, however, have wavelengths greater than 1000 Å, very large with respect to the orbit of the bound electron. The effect of such phonons on the lithium center should therefore be equivalent to that of time-varying long-range strains. We know from Eq. (12), however, that simple dilatation and the strains e_θ and e_ϵ do not couple the T_2z state with any of the other states (3), while our failure to alter the Li^7 interaction with large applied off-axis static shear strains rules out the possibility that any such coupling can result from the strains e_{yz}, e_{zx}, e_{xy}. A second possible explanation is that a local vibrational mode carries the lithium ion out of the node and thus gives it hyperfine interaction proportional to the square of the amplitude of vibration. Again, the linear temperature dependence would require $\hbar\omega/k\lesssim 2°K$ (1.4 cm^{-1}) for such a mode, an unreasonably low frequency for so light an atom. The frequency for this local mode of vibration for the isolated interstitial lithium ion in silicon has indeed been calculated by Bellomonte and Pryce[39] to be similar to the value 522 cm^{-1} found for the Li^7 ion (or 534 cm^{-1} for Li^6) in the lithium-boron pair complex.[40] As we will discuss below, our lithium hyperfine data provide further support for such an estimate of this frequency.

The third possibility is that in the electronic system we have a Boltzmann distribution between the ground state T_2z and the nearby excited state a_1', and that the lifetime of the excited state is short enough so that the

[39] L. Bellomonte and M. H. L. Pryce, Proc. Phys. Soc. (London) **89**, 967 (1966); **89**, 973 (1966).
[40] W. G. Spitzer and M. Waldner, J. Appl. Phys. **36**, 2450 (1965).

averaged hyperfine interaction, given by

$$A = A_z p_z + A_{a'} p_{a'}, \tag{42}$$

is observed.[41] Here A_z and $A_{a'}$ denote the hyperfine parameters of the lithium in the $T_2 z$ and a_1' states, respectively, and p_z and $p_{a'}$ are the corresponding occupation probabilities of these two states, so that we have

$$p_{a'}/p_z = \exp[-(E_{a'}-E_z)/kT]. \tag{43}$$

Using these equations, we have calculated the temperature dependence of the lithium hyperfine interaction, as shown in Fig. 12, for three different assumed values of $E_{a'}-E_z$, adjusting A_z and $A_{a'}$ in each case for the best fit. These values are given in Table I. We see that an excellent fit is achieved for $E_{a'}-E_z=0.48$ meV. The other choices for $E_{a'}-E_z$, representing $\pm 15\%$ deviation from this value, indicate the sensitivity of the fit to this choice.

Equation (42) also applies to the Si^{29} hyperfine interactions. Here, assuming as before that the resolved interactions arise from the planes with $|z| = \frac{1}{4}a_0$, we have

$$A_z/A_{a'} = \sin^2(\tfrac{1}{4}k_0 a_0)/\cos^2(\tfrac{1}{4}k_0 a_0) \simeq 17$$

for $k_0 = 0.85(2\pi/a_0)$. With this and Eqs. (42) and (43), the temperature dependence of the Si^{29} hyperfine interactions can also be calculated. The results are shown in Fig. 12 for $E_{a'}-E_z=0.48$ meV; the agreement is again seen to be excellent.[42]

From this determination of the energy difference $(E_{a'}-E_z)$ under stress, we can now obtain a value for the valley-orbit splitting $6\Delta_c$, if we assume (see Sec. VI) that the doublet and triplet states are degenerate in the absence of stress. Taking $\Xi_u = 11.4$ eV (as determined directly from our data in Sec. VII), we substitute the value for $x\Delta_c$ determined from Eqs. (27) and (29) using the known stress (470 kg/cm^2, corresponding to the data leading to Table I) into the expression

$$6\Delta_c = \frac{(E_{a'}-E_z)[(E_{a'}-E_z)+3x\Delta_c]}{[(E_{a'}-E_z)+x\Delta_c]} \tag{44}$$

obtained from the difference of Eqs. (30) and (31). The resulting values of $6\Delta_c$ and x are given in Table I. Also given in Table I is the value one obtains for A_0, the lithium hyperfine interaction parameter for the completely symmetric A_1 state in the absence of stress, using these values for x and $A_{a'}$ and the formula

$$A_{a'} = \tfrac{1}{2}[1-(2-\tfrac{1}{3}x)(x^2-\tfrac{4}{3}x+4)^{-1/2}]A_0. \tag{45}$$

This relation[5,29] follows from the fact that in the absence of stress only the A_1 singlet has a nonzero amplitude at the lithium nucleus; the contact hyperfine interaction in the a_1' state is therefore due to the admixture of the singlet into this state as a result of the stress.

Equations (31), (42), (43), and (45) also allow us to calculate the stress dependence of the Li^7 hyperfine splitting. Again with $\Xi_u = 11.4$ eV, and $6\Delta_c = 1.8$ meV, an excellent fit to the data is obtained at 1.66°K, as seen in Fig. 13. Also shown is the predicted dependence for values of $6\Delta_c$ of 1.8 ± 0.3 meV.

We conclude that the dependence of the Li^7 and Si^{29} hyperfine interactions upon temperature and stress is satisfactorily explained as the averaged value between the ground state $T_2 z$ and the nearby excited state a_1'. On the basis of our data alone, we conclude that the zero-stress valley-orbit splitting $6\Delta_c$ is 1.8 ± 0.3 meV. This value is in excellent agreement with the value 1.8 ± 0.1 meV estimated by Aggarwal *et al.*[7] on the basis of an energy difference between two resolved optical transitions, and our result serves to confirm their interpretation. Using the error estimate of Aggarwal *et al.* (1.8 ± 0.1 meV), we thus determine from Table I the hyperfine splitting A_0 for the singlet A_1 state at zero stress to be[43]

$$A_0/h = 2.3\pm 0.5 \text{ Mc/sec}. \tag{46}$$

In Table I and Fig. 12, we note that a small value for A_z, the lithium hyperfine interaction in the $T_2 z$ state, is possibly required for the best fit to the data. Although the $T_2 z$ wave function has a node at the interstitial lithium site, a small nonzero value for A_z would be expected if the zero-point vibration of the lithium ion carries it out of the node. If the vibrational frequency ν_{Li} of the lithium is of the order of 500 cm^{-1}, as estimated by Bellomonte and Pryce,[39] it is in fact reasonable to assume that the electronic states do not follow the lithium ion since the valley-orbit splitting of the electronic states is so much smaller (this is the reverse of the

TABLE I. Parameters deduced from fit of theory to temperature dependence of Li^7 hyperfine interaction, Fig. 12.[a]

$E_{a'}-E_z$ (10^{-3} eV)	A_z/h (Mc/sec)	$A_{a'}/h$ (Mc/sec)	x	$6\Delta_c$ (10^{-3} eV)	A_0/h (Mc/sec)
0.41	0	0.364	−7.0	1.48	1.61
0.48	0.004	0.470	−5.7	1.81	2.28
0.55	0.007	0.610	−4.7	2.18	3.28

[a] Values of x, $6\Delta_c$, and A_0 were deduced assuming $\Xi_u = 11.4$ eV.

[41] From the theory of the motional averaging of resonance lines (Ref. 26), the lifetime $\tau_{a'}$ of the excited state must be less than $h/\pi|A_{a'}-A_z|$ ($\simeq 7\times 10^{-7}$ sec from the data in the middle line of Table I), if the line corresponding to the averaged lithium hyperfine interaction (42) is to be observed rather than the lines corresponding to the individual states. Under these conditions, T_2 for the ENDOR lines is given theoretically [Ref. 26; see also Fig. 10 of G. D. Watkins and J. W. Corbett, Phys. Rev. **134**, A1359 (1964)] by $T_2 = [h^2/\pi^2 p_{a'} p_z^2 \tau_{a'}(A_{a'}-A_z)^2]$. Since an upper bound for $1/T_2$ is provided by the actual ENDOR linewidth Δf, we thereby deduce that $\tau_{a'} \leq [h^2\Delta f/\pi p_{a'} p_z^2 (A_{a'}-A_z)^2] \simeq (h/\pi A_{a'})(h\Delta f/A)$, where we have used Eq. (42) and the values $p_z \simeq 1$, $A_z \simeq 0$. From our data on the lithium ENDOR lines we find the ratio $(h\Delta f/A)$ to be roughly temperature independent in the range $2°K \lesssim T \lesssim 4°K$, with a value $\simeq 0.3$. We therefore deduce for the excited state lifetime under the conditions of stress appropriate to Fig. 12 the value $\tau_{a'} \leq 2\times 10^{-7}$ sec.

[42] Using an analysis similar to that of Ref. 41, we find that the Si^{29} ENDOR linewidths indicate $\tau_{a'} \lesssim 4\times 10^{-7}$ sec, a value consistent with our estimate from the lithium ENDOR linewidth.

[43] The estimate of error has been made large enough to include a substantial uncertainty in Ξ_u. See Sec. VII and Ref. 63.

usual situation, required for the validity of the Born-Oppenheimer approximation, in which the energy differences of the electronic states are much *larger* than the vibrational frequencies). The electronic states should then be centered on the average position of the lithium ion. Assuming the periodic parts $u_{\pm z}(\mathbf{r})$ of the Bloch functions to be approximately constant near the interstitial site, we have from Eqs. (3) or (37) that the expectation value for $|\Psi(\mathbf{r})|^2$ in the T_2z state at the instantaneous position of the lithium ion, averaged over the zero-point motion, is given by

$$\langle|\Psi(\mathbf{r})|^2\rangle_{\rm av}=2\eta_{\rm Li}|F(0)|^2|u_z(0)|^2k_0^2\langle z^2\rangle_{\rm av}. \quad (47)$$

Here we have approximated $\langle\sin^2k_0z\rangle_{\rm av}$ by $k_0^2\langle z^2\rangle_{\rm av}$ in view of the small excursion of the lithium ion from its average position, and we have introduced a parameter $\eta_{\rm Li}$ which is analogous to the parameter η in Eq. (39) but which represents the factor by which $|\Psi(\mathbf{r})|^2$ is enhanced at the lithium nucleus, above the value predicted by the effective-mass approximation, as a result of central-cell effects. We then approximate the local vibrational mode as involving only the motion of the lithium ion (that is, we neglect the coupled motion of the neighboring silicons), and we approximate the reduced mass of the mode by the lithium mass M. We have then for the zero-point average in the vibrational ground state the result

$$\langle z^2\rangle_{\rm av}=\hbar/4\pi M\nu_{\rm Li}. \quad (48)$$

Combining Eqs. (47) and (48) with Eq. (41), we thus obtain for the lithium hyperfine interaction in the T_2z state the result

$$A_z=(8/3)(\mu_{\rm Li}/I_{\rm Li})(\hbar k_0^2/M\nu_{\rm Li})\times\beta\eta_{\rm Li}|F(0)|^2|u_z(0)|^2. \quad (49)$$

On the other hand, in the singlet A_1 state we have from Eqs. (3) and (41)[44]

$$A_0=32\pi(\mu_{\rm Li}/I_{\rm Li})\beta\eta_{\rm Li}|F(0)|^2|u_z(0)|^2, \quad (50)$$

so that from Eqs. (49) and (50) we predict the ratio

$$A_z/A_0=\hbar k_0^2/12\pi M\nu_{\rm Li}, \quad (51)$$

which has the value $(0.77/\nu_{\rm Li})$ (for Li^7) if $\nu_{\rm Li}$ is given in cm^{-1}. Using the value (46) for A_0, we would thus have $A_z/h=3.5\times10^{-3}$ Mc/sec if we assume $\nu_{\rm Li}=500$ cm^{-1}. This value is in excellent agreement with the value $A_z=4\times10^{-3}$ Mc/sec obtained (Table I) from the best fit to Fig. 12. Conversely, if $\nu_{\rm Li}$ were as low as 100 cm^{-1}, we would predict from Eq. (51) a value $A_z/h=1.8\times10^{-2}$ Mc/sec which would be in clear disagreement with Fig. 12. As mentioned earlier, this result provides some support for the assumption that $\nu_{\rm Li}$ has a value ~500 cm^{-1}, as estimated by Bellomonte and Pryce.[39] It would of course be of interest to determine if A_z depends on the lithium isotopic mass, as predicted by Eq. (49). Such a determination could be made from a study of the ratio of Li^6 to Li^7 hyperfine splittings at $\lesssim1°K$, but this was not possible in our cryostat.

We want also to compare the value for the enhancement factor $\eta_{\rm Li}$ which we obtain from Eq. (50) using our experimental value (46) for A_0 with the value one can estimate theoretically. Taking $|F(0)|^2$ in Eq. (50) to be given by Eq. (35), and approximating $|u_z(0)|^2$ at the interstitial site by the average value of $|u_z(\mathbf{r})|^2$ over the unit cell, which in our units equals unity, we obtain, using the value (46), the experimental result

$$(\eta_{\rm Li})_{\rm expt}=34. \quad (52)$$

To obtain a thoretical estimate, we assume that the enhancement factor arises principally from the correction to the effective-mass wave function (1) which makes the resulting function orthogonal to the $1s$ core state of the lithium ion. If $\Psi(\mathbf{r})$ denotes the uncorrected effective-mass wave function for the A_1 singlet and if we approximate the lithium $1s$ state[20,39] by

$$\phi_{1s}=\alpha^{3/2}\pi^{-1/2}e^{-\alpha r}, \quad (53)$$

we have then for the corrected donor function

$$\Psi'(\mathbf{r})\simeq\Psi(\mathbf{r})(1-8e^{-\alpha r}), \quad (54)$$

where we have assumed in evaluating the integral $\int\Psi(\mathbf{r})\phi_{1s}\,d\tau$ that $\Psi(\mathbf{r})$ is constant over the region through which ϕ_{1s} extends. Setting $\mathbf{r}=0$ in Eq. (54) and forming $|\Psi'(0)|^2$, we find therefore for our theoretical estimate of the enhancement factor the result

$$(\eta_{\rm Li})_{\rm theor}=49. \quad (55)$$

In making this estimate, we have ignored all central-cell corrections other than the orthogonality correction, as for example, any increase in amplitude of the smooth part of $\Psi'(\mathbf{r})$ near the lithium that would result if the Coulomb attraction serves to accumulate more charge density in the central cell than is given by the effective-mass approximation. In view of the small central-cell corrections to the binding energy, it appears reasonable to assume that any such additional corrections to the wave function are also small. We have also ignored any exchange polarization of the lithium core. The theoretical estimate (55) is indeed in about as good agreement with the experimental value (52) as we ought to expect, given our various approximations. In particular, it is in substantially better agreement than an earlier very rough theoretical estimate by Kohn,[1,33] which gave

[44] We assume, as discussed later in the paper, that the enhancement factor $\eta_{\rm Li}$ in Eqs. (47)–(50) results principally from the correction to the effective-mass wave function (1) which is necessary to satisfy the requirement that the donor state be orthogonal to the $1s$ core state of the lithium ion in the instantaneous configuration of the ion as it vibrates. One may then show easily that the same factor $\eta_{\rm Li}$ enters both Eqs. (49) and (50). We are assuming, in effect, that even though the node in the T_2z wave function does *not* follow the vibrational motion of the lithium ion, the admixture of the $1s$ core state to the effective-mass state, which ensures the orthogonality, *does* follow that motion. This assumption appears reasonable since the energy difference between the core state and the valence state *is* large compared with the vibrational frequency.

$|\Psi'(0)|^2 \simeq 0.002 \times 10^{24}$ cm^{-3} corresponding to a value $\eta_{Li} \simeq 8$.

VI. SPECTRUM WITH DEGENERACY

A. Effect of Spin-Orbit Interaction

The independent-valley model of Sec. III B was not able to account for the spectrum at zero or low stresses, suggesting the presence of a small interaction between the valleys not included in the treatment. In this section we expand the treatment to include the effect of a small spin-orbit interaction coupling the nearly degenerate ground states of the lithium donor.

The general form which the spin-orbit interaction may take with respect to the states given by Eq. (3) for the ground hydrogenic manifold is fully determined by symmetry considerations in terms of two parameters λ and λ', if the site symmetry of the lithium ion is truly tetrahedral, as we shall assume (see Sec. VI C 3). We shall let λ determine the strength of the spin-orbit coupling within the triplet T_2, while λ' determines that of the coupling between the triplet and the doublet E. From tables[45] of the coupling coefficients for the group T_d, it follows that we can represent the spin-orbit coupling within these states by

$$\mathcal{H}_{so} = \lambda \mathfrak{L} \cdot \mathbf{S} + \lambda' \mathfrak{L}' \cdot \mathbf{S}, \tag{56}$$

where $\mathfrak{L}$ and $\mathfrak{L}'$ are imaginary Hermitian vector operators with components transforming by the irreducible representation T_1 of the tetrahedral symmetry group. We define $\mathfrak{L}$ such that it has nonzero matrix elements only among the triplet states given by

$$\begin{aligned} \langle T_{2y}|\mathfrak{L}_x|T_{2z}\rangle &= \langle T_{2z}|\mathfrak{L}_y|T_{2x}\rangle \\ &= \langle T_{2x}|\mathfrak{L}_z|T_{2y}\rangle = -i, \end{aligned} \tag{57}$$

while $\mathfrak{L}'$ has nonzero matrix elements only between the doublet and triplet:

$$\begin{aligned} &\langle E\epsilon|\mathfrak{L}_x'|T_{2x}\rangle = \langle E\epsilon|\mathfrak{L}_y'|T_{2y}\rangle = -\tfrac{1}{2}i, \\ &\langle E\theta|\mathfrak{L}_x'|T_{2x}\rangle = -\langle E\theta|\mathfrak{L}_y'|T_{2y}\rangle = -\tfrac{1}{2}i\sqrt{3}, \\ &\langle E\epsilon|\mathfrak{L}_z'|T_{2z}\rangle = +i. \end{aligned} \tag{58}$$

Let us assume that λ and λ' are small compared with the spin Zeeman splitting $\sim 2\beta H$, so that the spin-orbit interaction may be treated as a perturbation on the magnetic energy levels. That we then obtain positive g shifts varying as H^{-2} can be seen as follows: For simplicity consider the triplet state by itself. We assume that the random strain in the crystal causes the states T_{2x}, T_{2y}, T_{2z} to have energies Δ_x, Δ_y, and Δ_z in accord with Eq. (15). Neglecting for now the difference $(g_{\parallel} - g_{\perp})$ and taking $\hat{\zeta}$ along $\mathbf{H}$ as before, we have for the matrix elements of the Hamiltonian $\mathcal{H}_H + \mathcal{H}_S + \mathcal{H}_{so}$ among the states with $S_\zeta = +\frac{1}{2}$

$$\begin{bmatrix} \Delta_x + \frac{1}{2}g_0\beta H & -\frac{1}{2}i\lambda\zeta_z & \frac{1}{2}i\lambda\zeta_y \\ \frac{1}{2}i\lambda\zeta_z & \Delta_y + \frac{1}{2}g_0\beta H & -\frac{1}{2}i\lambda\zeta_x \\ -\frac{1}{2}i\lambda\zeta_y & \frac{1}{2}i\lambda\zeta_x & \Delta_z + \frac{1}{2}g_0\beta H \end{bmatrix}. \tag{59}$$

Among the states with $S_\zeta = -\frac{1}{2}$, the matrix elements are the same as in Eq. (59) except that the sign of $\frac{1}{2}g_0\beta H$ and of all the off-diagonal terms is reversed. Since the eigenvalues of the matrix (59) are real and thus independent of the sign of the imaginary off-diagonal terms, they have the same values relative to $+\frac{1}{2}g_0\beta H$ for the states with $S_\zeta = +\frac{1}{2}$ as they do relative to $-\frac{1}{2}g_0\beta H$ for the states with $S_\zeta = -\frac{1}{2}$. Thus to the accuracy of ignoring matrix elements of the spin-orbit interaction between states with $S_\zeta = +\frac{1}{2}$ and those with $S_\zeta = -\frac{1}{2}$, we have three pairs of states, each pair separated in energy by exactly $g_0\beta H$. This situation is illustrated in Fig. 14(b). If now we take account of the matrix elements of $\mathcal{H}_{so}$ between states of different S_ζ, and if we assume that the differences between Δ_x, Δ_y, Δ_z are also small relative to $g_0\beta H$, then the energy separation of the states of each pair is increased to the accuracy of second-order perturbation theory by an amount proportional to $\lambda^2/(g_0\beta H)$,

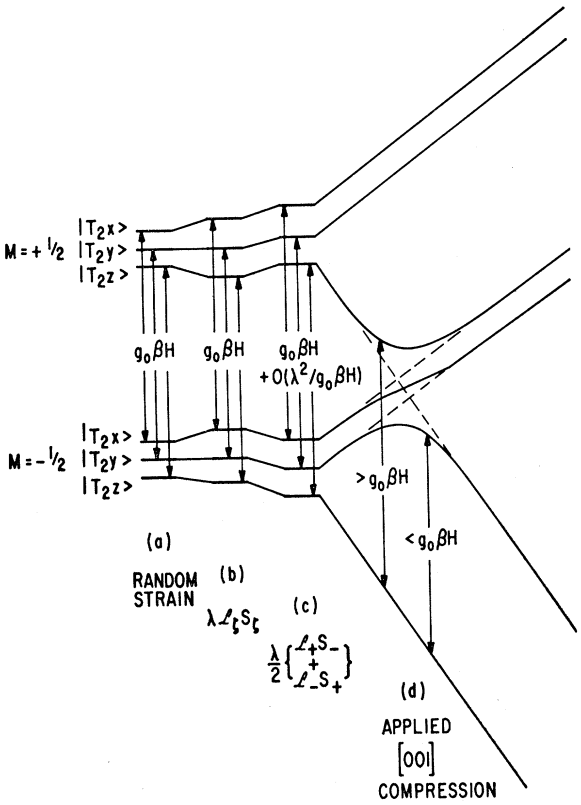

FIG. 14. Schematic drawing of the energy levels and allowed EPR transitions for three T_2 states. (a) Effect of random strain, $\Delta < g_0\beta H$; (b) diagonal, and (c) off-diagonal effects of spin-orbit interaction $\lambda < \Delta$ leading to positive g shifts $\sim \lambda^2/H^2$; (d) effect of applied [001] compressional stress, illustrating first the shift to greater positive g shifts and then the emergence at negative g-shift positions of the spectral lines.

[45] G. F. Koster, J. O. Dimmock, R. G. Wheeler, and H. Statz, *Properties of the Thirty-Two Point Groups* (M.I.T. Press, Cambridge, Mass., 1965).

as in Fig. 14(c). If spin transitions between the two states of each pair are allowed, they therefore occur for an apparent g value (defined by $g\beta H=h\nu$) shifted from g_0 by a small positive amount proportional to $\lambda^2/(g_0\beta^2H^2)$. If, furthermore, the typical differences between Δ_x, Δ_y, and Δ_z are larger than λ, these transitions between the two states of each pair (which then correspond to spin flips for a given orbital state) are more strongly allowed than transitions between states of different pairs. The frequencies for these latter transitions depend, moreover, on Δ_x, Δ_y, and Δ_z, so that in addition to being weak they will be broadened by the dependence of the Δ's on the random strain. Under these assumptions ($g_0\beta H>|\Delta_i-\Delta_j|>|\lambda|$), the EPR spectrum will therefore show only the three lines corresponding to the intrapair transitions, and these will have positive g shifts proportional to H^{-2}.

The theory now also accounts in a logical fashion for the behavior of the spectrum versus stress found in the low-stress transition region, as shown in Figs. 8–10. This can be seen from Fig. 14(d), which illustrates, again just for the T_2 states, the case for [001] compression. As stress is applied, some spin-up and spin-down states arising from different orbital states attempt to cross. Because of the spin-orbit coupling connecting them, they cannot cross, and a repulsion of levels occurs as shown in the figure. Because of this repulsion, the energy difference between the spin-up and spin-down states of each pair will increase as the crossover is approached, producing a shift to higher apparent g values. This is illustrated for the T_2z states in Fig. 14(d). Past the crossover, the same repulsion serves to decrease the energy splitting, giving negative g shifts. These shifts now decrease as the stress is further increased and the crossover is left behind. In the limit of large stress, where the orbital degeneracy of the ground state has been removed by $\gg g_0\beta H$, these g shifts approach 0.

From Eqs. (29) and (30), the crossovers will tend to occur when $\Xi_u e_\theta\sim g_0\beta H$. At 20 kMc/sec and with $\Xi_u=11.4$ eV and $(S_{11}-S_{12})=9.73\times10^{-13}$ cm^2 dyn^{-1},[46] Eqs. (27) and (28) give for this condition ~7.5 kg/cm^2 for [001] stress and ~15 kg/cm^2 for [110]. From Figs. 9 and 10 we see that the divergences of the g values are indeed centered roughly around these values.

Qualitatively, therefore, it appears that the inclusion of small spin-orbit coupling within the ground 1s hydrogenic manifold can account for the essential features of the zero- and low-stress EPR spectra. Let us proceed, therefore, to a quantitative test of the model in which we also include the doublet states.

In trying to make this model provide a quantitative description of the data, we find it necessary to assume that in zero applied stress the doublet states lie very close in energy to the triplet states, and that the energy differences of these five states in the random residual strain are now typically larger than both λ and λ' but again smaller than $g_0\beta H$. The situation is therefore qualitatively the same as that described in connection with Eq. (59), except that now we have five pairs of states, each of which gives rise to a spin transition corresponding to a g value which has been given a small positive shift proportional to H^{-2} by the spin-orbit coupling. We obtain on this basis for the triplet states T_2x, T_2y, T_2z, respectively, the g values (for zero applied stress)

$$\begin{aligned}
g_x&=g_0+\tfrac{1}{3}(g_{11}-g_1)(3\zeta_x^2-1)+(\lambda^2/2g_0\beta^2H^2)(1+\zeta_x^2)\\
&\quad+(\lambda'^2/2g_0\beta^2H^2)(1-\zeta_x^2),\\
g_y&=g_0+\tfrac{1}{3}(g_{11}-g_1)(3\zeta_y^2-1)+(\lambda^2/2g_0\beta^2H^2)(1+\zeta_y^2)\\
&\quad+(\lambda'^2/2g_0\beta^2H^2)(1-\zeta_y^2),\\
g_z&=g_0+\tfrac{1}{3}(g_{11}-g_1)(3\zeta_z^2-1)+(\lambda^2/2g_0\beta^2H^2)(1+\zeta_z^2)\\
&\quad+(\lambda'^2/2g_0\beta^2H^2)(1-\zeta_z^2),
\end{aligned}\tag{60}$$

where now we have included the difference $(g_{11}-g_1)$ to first order. For the combination of the doublet states which are eigenstates of the local strain, we have the states $E+$ and $E-$ given by Eq. (17), and corresponding to these the g values

$$\begin{aligned}
g_\pm&=g_0+(\lambda'^2/2g_0\beta^2H^2)\mp[1-3(\zeta_x^2\zeta_y^2+\zeta_y^2\zeta_z^2+\zeta_z^2\zeta_x^2)]^{1/2}\\
&\quad\times\cos(\psi-\alpha)\,[\tfrac{1}{3}(g_{11}-g_1)+(\lambda'^2/4g_0\beta^2H^2)].
\end{aligned}\tag{61}$$

In obtaining Eq. (61) we have used Eq. (22) and the angles ψ and α defined as in Eqs. (19) and (21). Because of the random character of the strain and therefore of the angle ψ, the two lines corresponding to $g_\pm$ are then broadened into a single line having a line shape given by Eq. (23) and Fig. 3. As we saw earlier, the edges of such a line are sharp, and they now correspond to g values

$$\begin{aligned}
g_\pm{}^*&=g_0+(\lambda'^2/2g_0\beta^2H^2)\\
&\quad\pm[1-3(\zeta_x^2\zeta_y^2+\zeta_y^2\zeta_z^2+\zeta_z^2\zeta_x^2)]^{1/2}\\
&\quad\times[\tfrac{1}{3}(g_{11}-g_1)+(\lambda'^2/4g_0\beta^2H^2)].
\end{aligned}\tag{62}$$

As before, relaxation between the E states can produce a lifetime averaging as indicated in Fig. 3, the averaged central line now emerging at

$$(g_\pm)_{\rm av}=g_0+(\lambda'^2/2g_0\beta^2H^2).\tag{63}$$

Absorption peaks in the EPR spectrum of Li in zero applied stress should thus occur at the five g values given by Eqs. (60) and (62), at temperatures sufficiently low that relaxation effects can be ignored. Rapid relaxation between the doublet states may cause the two lines of (62) to collapse into a single line (63). There is a limited range for the relaxation time over which the three lines due to the doublet may be simultaneously present.

Finally, we must obtain for this model the g values corresponding to the situation in which the degeneracy of the ground state has been lifted partially by tension applied along a cube direction, or equivalently by a uniaxial compression along a [110] direction. Taking the direction for the tension to be [001], we have according to Eq. (30) and Fig. 4 a triply degenerate (or very nearly

[46] H. J. McSkimin and P. Andreatch, Jr., J. Appl. Phys. **35**, 2161 (1964).

degenerate) ground state comprising the states T_2x, T_2y, and $E\epsilon$. Considering the splitting under the applied tension to be large so that we need consider only the g shifts due to matrix elements of the spin-orbit interaction (56) among these three states, and assuming as before that the energy differences of these states in the random residual strain is typically larger than λ and λ' but smaller than $g_0\beta H$, we obtain for the g values

$$g_x'=g_0+\tfrac{1}{3}(g_{\parallel}-g_{\perp})(3\zeta_x^2-1)+(\lambda^2/2g_0\beta^2H^2)(1-\zeta_x^2)+(\lambda'^2/8g_0\beta^2H^2)(1-\zeta_x^2), \quad (64a)$$

$$g_y'=g_0+\tfrac{1}{3}(g_{\parallel}-g_{\perp})(3\zeta_y^2-1)+(\lambda^2/2g_0\beta^2H^2)(1-\zeta_y^2)+(\lambda'^2/8g_0\beta^2H^2)(1-\zeta_y^2), \quad (64b)$$

$$g_\epsilon'=g_0-\tfrac{1}{6}(g_{\parallel}-g_{\perp})(3\zeta_z^2-1)+(\lambda'^2/8g_0\beta^2H^2)(1+\zeta_z^2). \quad (64c)$$

B. Comparison with Experiment

1. [110] Compression or [001] Tension

With tension along the [001] direction or compression along [110], we see from Eqs. (64a)–(64c) that for **H** parallel to [001] ($\zeta_x=\zeta_y=0$, $\zeta_z=1$) the g values for all three states T_2x, T_2y, and $E\epsilon$ depend on the spin-orbit interaction only through the parameter λ'. These formulas fit the data for this orientation quite well, as may be seen from Fig. 15(a), except that there is a small splitting of the T_2x and T_2y lines for which the model does not account. Ignoring this small splitting, we use this comparison with the predictions of Eq. (64) to identify the lines as shown in Fig. 15(a) and to determine a value $|\lambda'|=0.056$ cm^{-1} which together with the term in $g_{\parallel}-g_{\perp}$ in Eq. (64c) accounts quite well [Fig. 15(a)] for the angular variation of g_ϵ'. The angular variation of g_x' and g_y' in Eqs. (64a) and (64b) depends also on λ, and the solid curves in Fig. 15(a) have been drawn for the values

$$|\lambda'|=0.056 \text{ cm}^{-1}, \quad |\lambda|=0.021 \text{ cm}^{-1}. \quad (65)$$

The over-all fit is seen to be quite good.

The three lines corresponding to T_2x, T_2y, and $E\epsilon$ appear approximately equally intense at $T\sim1.5$°K, confirming that these three states are very nearly degenerate. The very close near-degeneracy of $E\epsilon$ with T_2x and T_2y is of course a condition for the presence of the λ' terms in Eq. (64) and their H^{-2} dependence (Fig. 7) since these terms arise only from the $E-T_2$ matrix elements of Eq. (58). We conclude, therefore, that the general features of the spectra for [110] compression or [001] tension can be satisfactorily described by the theory of the previous section when spin-orbit coupling both within the T_2 states (λ) and between the T_2 and the E states (λ') is required.

2. Zero Stress

With the values (65) for λ and λ', Eqs. (60), (62), and (63) can be used to predict the zero-stress spectrum. The result is shown by the solid and dashed lines in Fig. 15(b). Although detailed agreement with the experimental data has not been achieved, the general over-all behavior is roughly accounted for. The total spread of g values and their general angular dependence—for instance, the near coincidence of all the lines when **H** is along [111]—is as predicted. [A comparable degree of agreement is found with the data of Fig. 6(b), and it is therefore not included as a separate figure.]

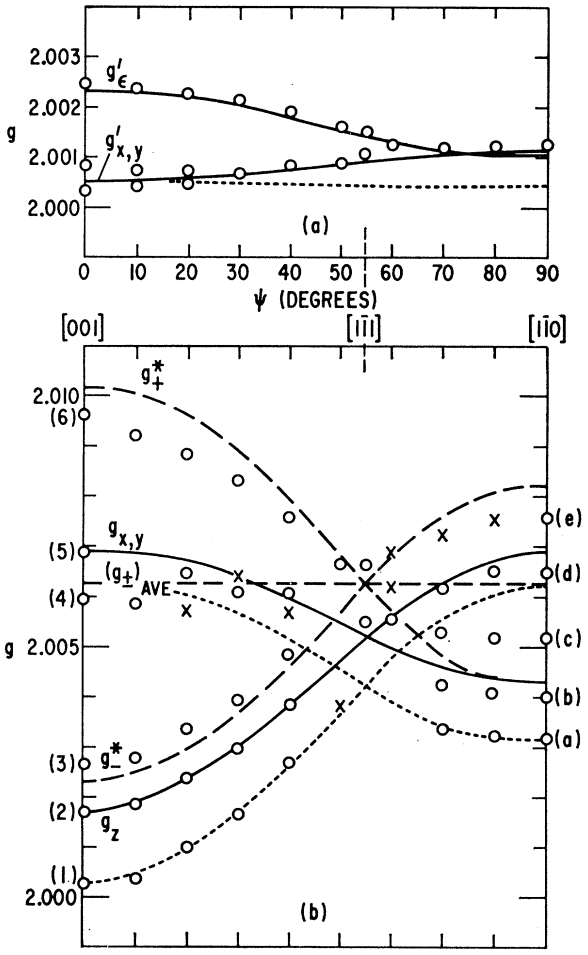

FIG. 15. Comparison of theory and observed EPR spectrum, **H** in the (110) plane: (a) large [110] compression; (b) zero stress. The solid and dashed lines are calculated for $|\lambda'|=0.056$ cm^{-1}, $|\lambda|=0.021$ cm^{-1}. The dotted curve is that calculated for the T_2 states if $|\lambda'|=0.056$ cm^{-1} and $|\lambda|=0.011$ cm^{-1}.

For a more detailed comparison, let us consider the E states first. For **H** along [001], lines 3 and 6 in Fig. 15(b) can be identified with the edges of the strain-broadened distribution as given by g_+* and g_-* in Eq. (62) and shown as a function of orientation by the dashed lines in the figure. The spectrum of Fig. 5(a) shows that these lines have the characteristic shape predicted in Fig. 3. The observed separation between the lines is slightly less than that between g_+* and g_-*, consistent with the predictions of Fig. 3 when a natural linewidth for the

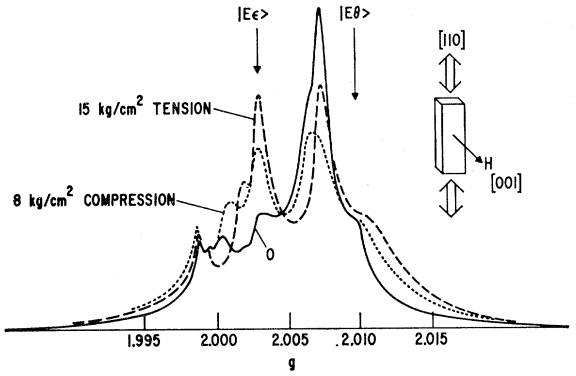

FIG. 16. Effect of small [110] stress on the EPR line shape for $H\|[001]$. The "peaking" at the position predicted for the $E\epsilon$ eigenstate serves to confirm the identification of the strain-broadened E-state line-shape components in the spectrum.

transitions is included. The disappearance of these lines as the temperature is raised can then be explained as resulting from a decrease in the relaxation time and the lifetime averaging as predicted in Fig. 3.

There are other qualitative features that tend to confirm this identification. A particularly convincing one is shown in Fig. 16. When we apply stress to the crystal, the strain distribution is, of course, no longer random. We would expect therefore to detect this as a change in the line shape for the E states. For example, with **H** along [001], the two edges of the random line shape correspond to the unmixed states $E\epsilon$ and $E\theta$, the $E\epsilon$ state giving the smaller g shift as shown in the figure. Stress along the [110] (or [001]) direction, therefore, should enhance the intensity of these edges because of the resulting concentration of the strain distribution along this [001] direction. There is the competing effect of the spin-orbit coupling to the reverse spin states as they try to cross under stress—the "crossovers" of Fig. 14—that tends to broaden and shift the lines at the same time and make this effect not so clean-cut. However, for the $E\epsilon$ state, Eq. (58) gives no coupling for this orientation of **H** to the $E\theta$ or T_2z states with opposite spin which it crosses, and the line should stay sharp and unshifted. This expectation is borne out dramatically in Fig. 16, the edge associated with this state increasing in intensity markedly and staying sharp and unshifted as stress is first applied. On the other hand, the $E\theta$ edge interacts with the T_2x and T_2y states that it attempts to cross, and the resulting broadening masks the peak enhancement due to the redistribution of the strain.

We note that line 4 in Fig. 15(b) is approximately symmetrically located between lines 3 and 6 and could be accounted for as the $(g_\pm)_{\rm av}$ line given by Eq. (63) and predicted in Fig. 3 for intermediate values of $K^{-1}\Delta g$. In order to match the general line shape seen at 1.5°K—e.g., the intensity of the $(g_\pm)_{\rm av}$ relative to that of lines 3 and 6—this interpretation would require $K^{-1}\Delta g\sim 5$. This in turn would give from Eq. (25) a value $\tau\simeq 4\times 10^{-8}$ sec at 1.5°K for the lifetime of the E states.[47]

With **H** along $[1\bar{1}0]$, the shape of the observed spectrum suggests that the lines marked c and e in Fig. 15(b) are also to be identified with the strain-broadened edges of the E state, consistent again with the predicted positions in the figure. We also note that line d is symmetrically located between them and may be identified with the $(g_\pm)_{\rm av}$ line.

The E states therefore appear to account satisfactorily for two, and perhaps three, of the lines in the zero-stress spectrum. At the same time, if we calculate g_x, g_y, and g_z for the T_2 states from Eq. (60), using the values (65), we obtain the solid curves in Fig. 15(b), which appear to account quite satisfactorily for two more of the lines. There remain, however, two lines—one terminating at line 1 for **H** along [001], the other in line a for **H** along $[1\bar{1}0]$—which are not accounted for by the theory.

The general angular dependence of these two remaining lines suggests that they also should somehow be associated with the T_2 states. In particular, if we take λ' as given by (65) but take instead for λ the smaller value $|\lambda|=0.011$ cm^{-1}, the dotted curves in Fig. 15(b) are then predicted for the T_2 states. The close agreement to the lower branches is suggestive, but of course if this explanation should be correct, the lines previously identified with the T_2 states would now not be accounted for. Moreover, the angular variation predicted for g_x' and g_y' under [110] compression now does not fit the data, as shown by the dotted line in Fig. 15(a).

We see, therefore, that by postulating a weak spin-orbit coupling among the nearly degenerate E and T_2 states, we are able to account rather well for the general magnitude of the observed g shifts in the zero-stress spectrum and the fact that they are all positive, for their field dependence as H^{-2}, and for their general angular dependence. However, our model has not yet succeeded in fitting all of the observed lines as accurately as we might wish, and what is worse, it apparently predicts fewer lines than are observed. There are a number of possible explanations for these discrepancies, as we will now discuss. Nevertheless, we are not able at the present time to make a compelling case in favor of any one of these possibilities, and for this reason we will not attempt to develop in detail any of these variants of our basic model. We must keep in mind, of course, that we really should not expect too close agreement between the predictions of our simple theory and the experi-

[47] This value for the lifetime of the states E^+ and E^- is roughly consistent with the theoretical estimate one obtains at 1.5°K by considering a one-phonon direct-process mechanism for transitions between the E states, using Eq. (16) ($\Xi_u=11.4$ eV) to provide the phonon coupling in the long-wavelength limit, and assuming the typical random strain splitting of the E states, as given by Eq. (18), to be $\sim$0.2 cm^{-1}. Moreover, according to these estimates the Orbach process through the singlet state dominates the relaxation process within the doublet above about 2°K and would account for the complete lifetime averaging of the doublet spectrum at higher temperatures, as observed.

mental data since there is, after all, considerable uncertainty in locating the positions of lines which are only barely resolved in the experimental spectra, as is clearly evident in Fig. 5. Moreover, as we will also discuss further below, the spectrum is dependent upon the residual strains which are present in the crystal, and these may shift the lines or perhaps introduce additional peaks in ways which our simplified treatment has not anticipated. In view of such uncertainties, as well as the difficulty in giving a complete analysis of this complicated system, we can be reasonably satisfied with our simple model, despite its shortcomings, as accounting for the essential features of the observed spectrum.

One possible explanation to account for extra lines in the zero-stress spectrum is that the lithium atom is displaced out of the interstitial tetrahedral position. If such a displacement were in a ⟨100⟩ direction, the site symmetry would be reduced from T_d to C_{2v}, and the spin-orbit coupling could be anisotropic with three independent parameters replacing both λ and λ'. Such a distortion can also couple to the electronic states, lifting the degeneracy of both the T_2 and E states and perhaps mixing these states. For our model to work at all (i.e., in order that the g shifts vary as H^{-2}), any such energy differences must be small with respect to $g_0\beta H$, and our earlier success in fitting the lines attributed to the E states to the random-strain model indicates that energy differences due to random strains probably dominate any such energy splittings due to a displacement of the lithium. Nevertheless, if such splittings are appreciable compared with the strain splittings, they might still cause displacements or splittings of the experimental resonance lines.

We have carried out a number of exploratory calculations making various assumptions for the model of a displaced lithium ion. The results of one particularly simple choice of parameters is shown in Fig. 17. Here, the lithium is taken to be displaced along a ⟨100⟩ direction, the notation X_y indicating the T_2x state associated with a lithium displacement in the $\pm y$ direction, etc. We have taken λ' to be isotropic, and λ to be symmetric about the axis of displacement, with $|\lambda'| = 0.056$ cm^{-1}, $|\lambda_{\parallel}| = 0.021$ cm^{-1}, $|\lambda_{\perp}| = 0.011$ cm^{-1}. This value for λ' is the same as that used before, while those for $\lambda_{\parallel}$ and $\lambda_{\perp}$ are equal to the values for λ which we found earlier served to fit one or the other pair of lines in the zero-stress spectrum which we associated with the T_2 states. We have assumed that the energy differences among the electronic states as a result of the random strains dominate any splittings due to the lithium displacement, so that these states are the same as those we had in Fig. 15(b). However, all six ⟨100⟩ displacements will now be simultaneously present, at least for zero applied stress, so that there are now more lines corresponding to these differently oriented centers, as shown by the curves in Fig. 17(b). As seen from Fig. 17(b), we are now able to account for the correct number of lines, which we could not do with the undisplaced model; the agreement between the individual lines which are predicted for the T_2 states and those which are observed is, however, not as good as it was in Fig. 15(b). To account for the data with compression along [110], we must now assume that under such an applied stress the displacements along $\pm z$ are preferentially selected. This assumption allows a fit to the data in Fig. 17(a) identical to that in Fig. 15(a) because the g shifts for X_z and Y_z under these conditions of stress involve $\lambda_{\parallel}$ but not $\lambda_{\perp}$.

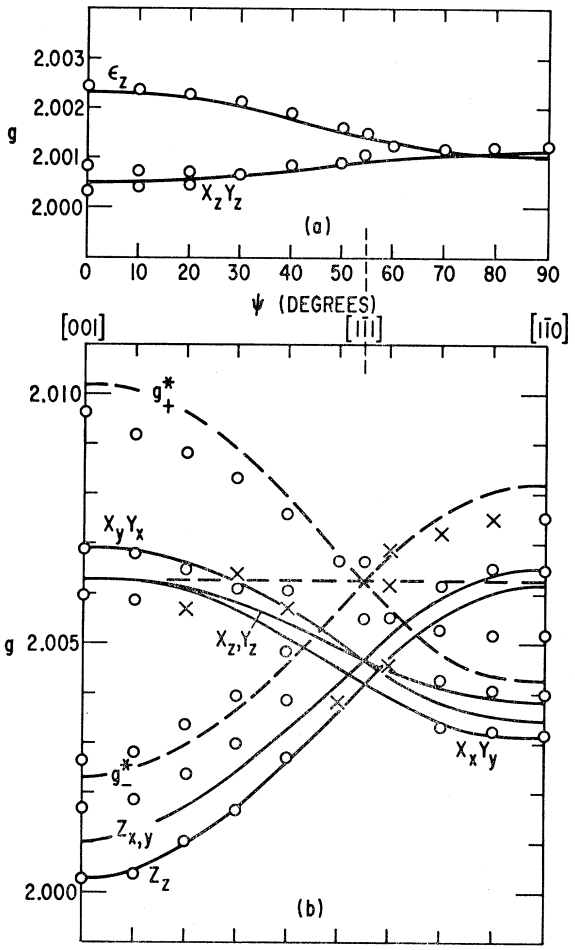

FIG. 17. Comparison of theory and observed EPR spectrum for a ⟨100⟩ displaced lithium model H in the (110) plane. The curves are calculated for $|\lambda'| = 0.056$ cm^{-1}, $|\lambda_{\parallel}| = 0.021$ cm^{-1}, $|\lambda_{\perp}| = 0.011$ cm^{-1}. X_y denotes the T_2x state for a lithium displacement in the $\pm y$ direction, etc. (a) Large [110] compression which has preferentially selected the $\pm z$ distortion; (b) zero stress.

It is clear from the results shown in Fig. 17 that a static displacement of the lithium out of the tetrahedral position can cause the kind of changes in the spectrum which are required—e.g., the "doubling" of the lines resulting from the T_2 states. Extending the treatment beyond that considered in Fig. 17 to include further anisotropies and/or appropriate mixing of the electronic states presumably might somewhat improve the

agreement with the experimental spectrum. Whether or not detailed agreement could be achieved in this way is not clear. Our limited attempts in this direction have not succeeded in greatly improving the agreement over that shown in Fig. 17.

One way in which we could double the number of lines attributed to the T_2 states while preserving the good agreement with the individual lines shown in Fig. 15(b) would of course be to postulate that two distinct configurations are available to the lithium ion—one for each set of (apparently isotropic) spin-orbit parameters. These two configurations would have to have almost precisely the same energy, in the absence of stress, to account for the simultaneous presence of both in the low-temperature spectra, and the requirement of an accidental equivalence in the energy of two such different configurations is of course a major weakness of this model. External stress would then have to preferentially select one of the configurations {for [110] compression the one with the larger value of λ, in order to account for the results in Fig. 15(a)}. This model would require, of course, that the lithium be able to change from one configuration to the other even at these low temperatures. Since it is not clear what two configurations we might have that would satisfy all these requirements, we do not consider this model a likely one.

C. Discussion

1. Magnitude of Splittings Caused by Random Strains

In order to be able to account as well as we have for the principal features of the observed spectrum, it was necessary to postulate that

$$g_0\beta H > \Delta > \lambda, \lambda', \tag{66}$$

where Δ is a representative value for the random strain splitting of the electronic states. Having now estimated λ and λ', we can return to this postulate to see if it is reasonable. At 20 kMc/sec we must then have

$$0.67\ \text{cm}^{-1} > \Delta > 0.056\ \text{cm}^{-1}, \tag{67}$$

which requires $\Delta \sim 0.1$ to 0.2 cm^{-1} or, from Eqs. (15) and (18) with $\Xi_u = 11.4$ eV, an rms strain

$$\langle e_\epsilon \rangle_{\text{rms}} \sim \langle e_\theta \rangle_{\text{rms}} \sim (1\text{–}2) \times 10^{-6}. \tag{68}$$

This is not an unreasonable value for the internal strain in a good crystal such as silicon, and we conclude, therefore, that our model is consistent.

The limits presented by the inequality (67) are, however, tight. Clearly we have been lucky that the various terms have happened to fall in the right place to allow our simple analysis. At the same time, we also realize that these narrow limits necessarily put restrictions on the accuracy of our calculated spectra and therefore on the agreement with experiment that we should expect. To explore this point further, consider the effect on the g values if Δ cannot be ignored with respect to $g_0\beta H$. If in the perturbation treatment leading to Eq. (60) the Δ_i's had been included in the energy denominators, the result for a typical g value would have been

$$\begin{aligned} g_x = g_0 &+ \tfrac{1}{3}(g_{\parallel} - g_{\perp})(3\zeta_x^2 - 1) \\ &+ (\lambda^2/2g_0\beta^2H^2)\left\{\frac{1-\zeta_z^2}{1-\delta_{xy}^2} + \frac{1-\zeta_y^2}{1-\delta_{xz}^2}\right\} \\ &+ (\lambda'^2/4g_0\beta^2H^2)(1-\zeta_x^2)\left\{\frac{1-\cos(\psi+\frac{1}{3}\pi)}{1-\delta_{x+}^2}\right. \\ &\left. + \frac{1+\cos(\psi+\frac{1}{3}\pi)}{1-\delta_{x-}^2}\right\}. \end{aligned} \tag{69}$$

Here $\delta_{ij} = (\Delta_i - \Delta_j)/g_0\beta H$; ψ is defined in Eq. (19); and Δ_+ and Δ_- denote the energies of the states $|E+\rangle$ and $|E-\rangle$. Equation (69) reduces to the corresponding Eq. (60) when we neglect the δ_{ij}^2. Since the δ_{ij} depend upon the random strain, it is clear from Eq. (69) that they serve to broaden the lines. In addition, because they appear quadratically, they serve to shift the lines. This shift corresponds to a fractional increase in the g shift of $\sim\langle\delta_{ij}^2\rangle_{\text{av}}$, which for $\Delta \sim 0.3 g_0\beta H$ would correspond to a change of $\sim 10\%$ in the g shift.

Errors in our treatment also exist because the assumption $|\Delta_i - \Delta_j| \gg \lambda, \lambda'$ is evidently not particularly well fulfilled. If two states with the same spin S_ζ have an energy difference $(\Delta_i - \Delta_j)$ which is comparable with the matrix element of $\lambda \mathfrak{L}_\zeta S_\zeta$ or $\lambda' \mathfrak{L}_\zeta' S_\zeta$ between them, the spin-orbit coupling will mix these states. For the reasons noted in Sec. VI A, we would not expect this mixing to change the number of resonance transitions exhibiting an H^{-2} variation in their g shifts, but the precise value of the g shifts will depend upon the particular admixture of the states. Again we obtain a broadening of the lines because of the dependence of the $\Delta_i - \Delta_j$ on the random strains, but we can also get errors in this way in the average position of the lines. For this reason, together with the others noted previously, we conclude that we should not expect too close a fit for our simple theory and that the agreement we have obtained is about as good as we ought to expect.

2. Origin of Spin-Orbit Interaction

A spin-orbit interaction has been identified earlier in the $1s(T_2)$ triplet state of the shallow donors P, As, Sb, and Bi in silicon. For the Bi donor, it was found by Krag and Zeiger,[48] from their observation of the $1s(A_1) \rightarrow 1s(T_2)$ optical transition, that the $1s(T_2)$ state was split into two levels with a separation of 1 meV. A similar splitting of 0.3 meV of the $1s(T_2)$ state of the Sb donor was inferred by Aggarwal and Ramdas[19] from their optical studies. Roth[49] first suggested that this splitting of the triplet was due to the spin-orbit interac-

[48] W. E. Krag and H. J. Zeiger, Phys. Rev. Letters **8**, 485 (1962).
[49] L. M. Roth, M.I.T. Lincoln Laboratory, Solid State Research Report No. 3, 1962, p. 23 (unpublished).

tion [in which case the splitting is $\frac{3}{2}\lambda$ in terms of the parameter we introduced in Eq. (56)], and she showed for Bi that the observed splitting was of the correct size to be plausibly attributed to the residual spin-orbit interaction of the ionic potential of the Bi impurity. Castner[50] subsequently showed that he could account quite satisfactorily for the measured rate constants in the Orbach contribution to the spin-lattice relaxation of the donor electron for the P, As, Sb, and Bi donors if he assumed a spin-orbit interaction in the $1s(T_2)$ state which is scaled down by a factor of roughly 5×10^{-4} (the same factor that gives the observed splitting for the Bi and Sb donors) from the atomic spin-orbit interaction of a valence p electron on the impurity atom.

One thus obtains values for λ of 0.1, 0.7, 1.6, and 5 cm^{-1} for P, As, Sb, and Bi, respectively, from these peterminations of the spin-orbit splitting of the $1s(T_2)$ state of these other shallow donors in silicon. Although these values are all much larger than the value $|\lambda|\simeq0.01-0.02$ cm^{-1} which we have obtained in our work for the $1s(T_2)$ state of the Li donor, it is clear that we cannot account for this interaction in a similar way as the residual effect of the impurity spin-orbit interaction. The spin-orbit splitting of the $2p\ ^2P^o$ state of the Li atom[51] is only 0.337 cm^{-1}, so that using a reduction factor $\sim5\times10^{-4}$ we would estimate on this basis a value for λ of only $\sim1\times10^{-4}$ cm^{-1}. Moreover, we could not explain in this way why we should find a value for $|\lambda'|$ *larger* than that for $|\lambda|$ since if spin-orbit interaction between the $1s(E)$ and $1s(T_2)$ states were are sidual atomic effect, it would have to trace its origin to the spin-orbit interaction of the d states of the Li atom instead of the p states. The spin-orbit splitting ~0.04 cm^{-1} of the $3d\ ^2D$ state[52] of atomic Li is, of course, very much too small to make any such explanation a possibility.

We are forced, therefore, to conclude that the small spin-orbit interactions which we have found in the $1s(T_2)$ state and between the $1s(T_2)$ and $1s(E)$ states of the Li donor must be due to the spin-orbit interaction of the host silicon crystal rather than to that of the Li impurity. To attempt a rough estimate for this contribution, consider the spin-orbit interaction $\mathcal{H}_{\text{so}}{}^h$ of an electron in the potential $V_h(\mathbf{r})$ of the host silicon crystal. This takes the form

$$\mathcal{H}_{\text{so}}{}^h=\frac{-e\hbar}{2m^2c^2}(\boldsymbol{\nabla}V_h\times\mathbf{p})\cdot\mathbf{S}, \tag{70}$$

where $\mathbf{p}$ is the electron momentum. Making use of the effective-mass approximation, we have the wave functions of our donor states given by Eqs. (1)–(3); we see from Eqs. (56)–(58) that the matrix elements that serve for the evaluation of λ and λ' are then proportional to off-diagonal matrix elements of $\mathcal{H}_{\text{so}}{}^h$ with respect to the effective-mass wave functions $\chi_j(\mathbf{r})$ associated with band minima on different axes. If we assume that there is no lattice distortion about the interstitial Li, $V_h(\mathbf{r})$ has the periodicity of the crystal, so that $\mathcal{H}_{\text{so}}{}^h$ in Eq. (70) is diagonal with respect to $\mathbf{k}$. Introducing the Fourier transform $G_j(\boldsymbol{\kappa})$ of the envelope function $F_j(\mathbf{r})$

$$G_j(\boldsymbol{\kappa})=(2\pi)^{-3/2}\int d\tau\,\exp(-i\boldsymbol{\kappa}\cdot\mathbf{r})F_j(\mathbf{r}), \tag{71}$$

we find therefore that the appropriate matrix elements of $\mathcal{H}_{\text{so}}{}^h$ are given by integrals over k space which contain in the integrand the products

$$G_n{}^*(\mathbf{k})G_m(\mathbf{k}+\Delta\mathbf{k}_{nm}+\mathbf{K}_N),$$

where $\Delta\mathbf{k}_{nm}=\mathbf{k}_0{}^n-\mathbf{k}_0{}^m$ is the separation in k space between the band minima n and m, while $\mathbf{K}_N$ is a vector of the reciprocal lattice. Because the transforms $G_j(\boldsymbol{\kappa})$ diminish rapidly in amplitude as $|\boldsymbol{\kappa}|$ increases from zero, the overlap of $G_n(\mathbf{k})$ with $G_m(\mathbf{k}+\Delta\mathbf{k}_{nm}+\mathbf{K}_N)$ is small for all possible $\mathbf{K}_N$, and these matrix elements determining λ and λ' are therefore small. We find, for example, for a typical such matrix element the result

$$\langle\chi_{+x}|(\boldsymbol{\nabla}V_h\times\mathbf{p})_z|\chi_{+y}\rangle$$
$$=\sum_N\int d\mathbf{k}\,G_{+x}{}^*(\mathbf{k})G_{+y}(\mathbf{k}+\Delta\mathbf{k}_{xy}+\mathbf{K}_N)U(\mathbf{k},\mathbf{K}_N), \tag{72}$$

where $U(\mathbf{k},\mathbf{K}_N)$ is an integral over a single unit cell of the silicon lattice given by

$$U(\mathbf{k},\mathbf{K}_N)$$
$$=\Omega_0{}^{-1}\int_{\text{cell}}d\tau\,\exp[-i(\mathbf{k}+\mathbf{k}_0{}^{+x})\cdot\mathbf{r}]u_{+x}{}^*(\mathbf{r})(\boldsymbol{\nabla}V_h\times\mathbf{p})_z$$
$$\times\exp[i(\mathbf{k}+\mathbf{k}_0{}^{+x})\cdot\mathbf{r}]\exp(i\mathbf{K}_N\cdot\mathbf{r})u_{+y}(\mathbf{r}), \tag{73}$$

and Ω_0 is the volume of the unit cell. If we assume that $U(\mathbf{k},\mathbf{K}_N)$ is approximately independent of $\mathbf{k}$, the matrix element (72) may be expressed in terms of $U(\mathbf{k},\mathbf{K}_N)\approx U(\mathbf{K}_N)$ if we evaluate the integral

$$W_{x,y}(\mathbf{K}_N)$$
$$=\int d\mathbf{k}\,G_{+x}{}^*(\mathbf{k})G_{+y}(\mathbf{k}+\Delta\mathbf{k}_{xy}+\mathbf{K}_N)$$
$$=\int d\tau\,\exp[-i(\Delta\mathbf{k}_{xy}+\mathbf{K}_N)\cdot\mathbf{r}]F_{+x}{}^*(\mathbf{r})F_{+y}(\mathbf{r}). \tag{74}$$

Neglecting for simplicity the anisotropy in $F_j(\mathbf{r})$ as given by Eq. (35) and introducing $a^*=n(a^2b)^{1/3}=19.4\times10^{-8}$ cm, we obtain

$$W_{x,y}(\mathbf{K}_N)=[1+\tfrac{1}{4}|\Delta\mathbf{k}_{xy}+\mathbf{K}_N|{}^2a^{*2}]^{-2}. \tag{75}$$

This has the value 3.0×10^{-5} for $\mathbf{K}_N=0$, while if we take

[50] T. G. Castner, Phys. Rev. **155**, 816 (1967).
[51] D. A. Jackson and H. Kuhn, Proc. Roy. Soc. (London) **A173**, 278 (1939).
[52] *Atomic Energy Levels*, edited by C. E. Moore, Natl. Bur. Std. (U. S.) Circ. No. 467 (U. S. Government Printing Office, Washington, D. C., 1949), Vol. I, p. 8.

the value for $\mathbf{K}_N$ which gives $|\Delta\mathbf{k}_{xy}+\mathbf{K}_N|$ its smallest possible value, we obtain for (75) a value 5.7×10^{-5}. If the value of $(e\hbar/2m^2c^2)U(\mathbf{K}_N)$ were of the same size as the matrix elements[53] of the spin-orbit interaction with respect to the Bloch states at $\mathbf{k}=0$ in the valence band which are responsible for the 350-cm^{-1} splitting in this band for silicon [this is undoubtedly too large an estimate for $U(\mathbf{K}_N)$, since the Bloch functions at $\mathbf{k}=0$ in the valence band are mainly $3p$ functions on the silicon atoms while there is a large s component in the conduction band], it then would follow that we could account for values of the matrix element (72) on the order 10^{-2} cm^{-1}. Although the rough agreement of these estimates with what is required to account for the observed values for λ and λ' is perhaps encouraging, it is clear that these quantitative arguments based on the effective-mass approximation cannot be taken too seriously. We know, of course, that the effective-mass approximation is inaccurate in representing those components of the donor wave function which vary rapidly from one silicon atom to another, but it is precisely such components having $|\mathbf{k}|\sim\frac{1}{2}|\Delta\mathbf{k}_{nm}+\mathbf{K}_N|$ which are represented by $G_j(\mathbf{k})$ in the region in k space where the integral (74) receives its principal contribution. We therefore cannot expect to calculate λ and λ' accurately from the effective-mass approximation. On the other hand, it would be exceedingly difficult to improve upon the effective-mass approximation to represent the wave function more accurately on the silicon atoms in the first few shells surrounding the Li—the shells which evidently account for the contribution to λ and λ'. We will not attempt any such calculation, which would have to consider also the possiblity that the nearby silicon atoms are slightly displaced as a result of the presence of the Li. We believe, nevertheless, that the arguments we have presented make it quite reasonable to attribute values for λ and λ' in the range 0.01–0.06 cm^{-1} to the effect of the spin-orbit interaction of the silicon atoms, as our earlier consideration of the impurity spin-orbit interaction indicated must be the case.

3. *Symmetry of Lithium Site*

The tetrahedral site is not necessarily the most stable one for an interstitial ion in the silicon lattice. Indeed, in his theory of the diffusion of interstitial ions in silicon, Weiser[9] has calculated that for lithium the hexagonal site is more stable than the tetrahedral site by $\simeq$0.5 eV, an energy difference that agrees well with the measured activation energy for lithium diffusion. Weiser found in his calculations that the electrostatic polarization energy dominates the energy of overlap repulsion, so that the hexagonal site with its six silicon neighbors is favored over the tetrahedral site. In contrast, Bellomonte and Pryce[39] concluded that the overlap repulsion dominates and that the tetrahedral site is therefore favored because of the lower density there of the silicon valence electrons. Nara and Morita[20] in turn found in their calculations that the hexagonal site favors the inverted valley-orbit splitting which is obtained experimentally, while the tetrahedral site gives a somewhat different splitting.

The EPR data now enable us to conclude that the lithium is definitely *not* in the hexagonal site. This site has point group symmetry D_{3d}, and in particular, it is a center of inversion symmetry. The eigenstates of an ion in this site accordingly have definite parity, and there can be no nonzero matrix elements of the spin-orbit interaction between such states of opposite parity. Of the linear combinations (3) of the effective-mass states for such an ion, the states A_1, $E\theta$, and $E\epsilon$ are even under inversion in the impurity site, while the T_2 states are odd. If the lithium were in the hexagonal site, therefore, the spin-orbit parameter which we have called λ' would be required by symmetry to be 0. We have seen that our data can be accounted for only if a nonzero value for λ' given by Eq. (65) is assumed. We conclude, therefore, that while this result is consistent with the lithium being in the tetrahedral site,[54] it rules out the possibility of the hexagonal site.

Apart from this consideration there is also other evidence from our EPR data which favors the tetrahedral site. If the lithium were in the hexagonal site, the trigonal symmetry of that site would be expected to show up, on one hand, in an anisotropic spin-orbit interaction (which, as we argue, arises from the neighboring silicon atoms and should therefore reflect the local symmetry) among the three T_2 states, and on the other hand as a splitting of the T_2 orbital triplet into a singlet and a doublet. Any such splitting would of course have to be smaller than $g_0\beta H$ in order not to disturb the H^{-2} variation of our g values shown in Fig. 7. If such a splitting were nevertheless present and larger than the splittings due to random strain, one can show that the g values of the resulting states should show an anisotropy indicative of the trigonal symmetry of the individual sites. In particular, some of the resonance frequencies should take their extreme values when $\mathbf{H}$ is along a $\langle111\rangle$ direction, and there is no indication of any such behavior in our data [see, for example, Fig. 15(b)]. Moreover, corresponding resonances arising from centers with different $\langle111\rangle$ directions for the trigonal symmetry axis are nevertheless equivalent when $\mathbf{H}$ is along a cube direction. The spectrum as in Fig. 15(b) would therefore be expected to have lines which split as $\mathbf{H}$ is rotated out of

[53] L. Liu, Phys. Rev. 126, 1317 (1962).

[54] The tetrahedral site is, of course, not a center of inversion, so that the A_1, E, and T_2 states for an ion in this site do *not*, in general, have a definite parity. The spin-orbit coupling between the E and T_2 states may accordingly be nonzero in this symmetry. For example, the T_2 states may involve linear combinations of p and d atomic functions on the impurity site, so that a nonzero value for λ' could result from the impurity spin-orbit interaction among the d states. Alternatively, since the silicon spin-orbit interaction (70) is not invariant with respect to inversion in the tetrahedral site, this can lead directly as in Sec. VI C 2 to nonzero matrix elements between E and T_2 states even if these states should be predominantly of opposite parity.

a ⟨100⟩ direction, again contrary to what we find. Similarly, if the trigonal splitting of the states were smaller than that due to random strain, but the spin-orbit interaction were anisotropic, we would again expect corresponding lines from differently oriented hexagonal sites to coincide for **H** in a cube direction and otherwise to show a splitting. Our data thus provide no evidence for the departures from cubic symmetry that one would expect if the lithium were in the hexagonal site.

In the analysis we have given in this paper, we have assumed that the site symmetry of the lithium is tetrahedral, apart from the effects of random strain, and as we have seen our experimental results are generally consistent with this assumption. There are some discrepancies, nevertheless, which led us to consider the possibility that the lithium might be displaced out of the tetrahedral site to a position of lower symmetry. While there was some indication from our data that such displacements may occur, our evidence for them was not compelling. We cannot, of course, rule out the alternative possibility that the lithium is displaced out of the hexagonal site, and indeed Weiser[9] has noted that such a displacement is favored by the polarization energy. Nevertheless, we would find it strange if a displacement from the hexagonal site could produce so large an effect on the spin-orbit interaction (i.e., the large value for λ') without causing some evident departure from the apparent tetrahedral symmetry of the resonance spectrum of each individual defect.

We conclude, therefore, that the lithium is definitely not in the hexagonal site and that it is more probably in the tetrahedral site, although it may possibly be displaced slightly out of the latter.

4. *Vibronic Effects*

The fact that the EPR spectrum was found to be the same for Li^6 and Li^7 indicates that there are no major vibronic effects involving the motion of the lithium ion. Were any such effects important, they might have shown up, as in the dynamic Jahn-Teller effect,[10,11] as a coupling between the electronic states and the vibrational motion of the lithium, with no loss in the effective symmetry of the defect but with parameters of the EPR spectrum depending on the vibrational frequency and thus on the lithium mass. Or, if this coupling were sufficiently strong, these effects might have appeared as in the static Jahn-Teller effect as a spontaneous distortion of the defect to a configuration of low symmetry in which the orbital electronic degeneracy of the ground state of the defect is removed. In this latter case, the EPR spectrum at the lowest temperatures should have been the superposition of the spectra corresponding to a simple spin flip in the orbitally nondegenerate ground state of each of these distorted configurations; in particular, the effect of the spin-orbit interaction which led to our H^{-2} variation in the g factors would have been quenched by the distortion. In the former dynamic case, the vibronic states of the coupled system would have associated somewhat different vibrational states of the lithium with the several electronic states, so that the matrix elements of the spin-orbit interaction would have been reduced in proportion to the vibrational overlap between the different states.[10] Since this vibrational overlap depends on the ratio of a coupling energy (the analog of the Jahn-Teller energy) to the energy of the vibrational mode, we would thus expect in particular that the H^{-2} variation in the g factors would have exhibited an isotopic mass dependence if this vibronic coupling were important.

The absence of any important vibronic effect involving the lithium motion in the EPR spectrum is what we might expect. The spread of the donor wave function over many cells of the silicon lattice means that the electronic states are only weakly coupled to the displacement of any single ion, whereas a significant vibronic effect requires a fairly strong coupling, like that found in various Jahn-Teller systems[11] in which the electronic states are localized on one or at most a few atoms. We may conclude also that, if the lithium is displaced out of the symmetrical site as our data indicate might possibly be the case, this displacement is then not the result of a Jahn-Teller-type coupling involving the donor electronic state (in which case the H^{-2} g-factor variation would have been quenched, as noted above), but rather must be the consequence of the instability of the Li^+ core in the symmetrical configuration. If such a displacement does occur, the data show that the electronic degeneracy of the donor state is thereby unaffected to within the splitting due to residual strains, so that any such coupling to the donor state is very small indeed.

Finally, we must estimate the contribution of the vibronic coupling with the silicon lattice to the valley-orbit splitting of the donor states. The calculation of this effect is a straightforward application of the theory of a dynamic Jahn-Teller effect,[19] and at first sight the effect appears possibly to be large because of the strong coupling of the donor states to a uniform strain. However, the large spatial extent of the donor states means that only phonons of very long wavelength are effective in the coupling. Since the strain field associated with a phonon of propagation vector $\mathbf{q}$ varies spatially as $\exp(i\mathbf{q}\cdot\mathbf{r})$, we find that the coupling is proportional to the integral

$$\int d\mathbf{r}\,|F_j(\mathbf{r})|^2 \exp(i\mathbf{q}\cdot\mathbf{r}) = [1+(\tfrac{1}{2}qa^*)^2]^{-2}, \quad (76)$$

where we have neglected the anisotropy of $F_j(\mathbf{r})$ in Eq. (35) and have introduced the average effective Bohr radius $a^*=n(a^2b)^{1/3}$. Calculating the energy displacement $\delta E(T_2)$ of the electronic triplet state T_2 as a result of the Jahn-Teller coupling to the acoustic phonons, we

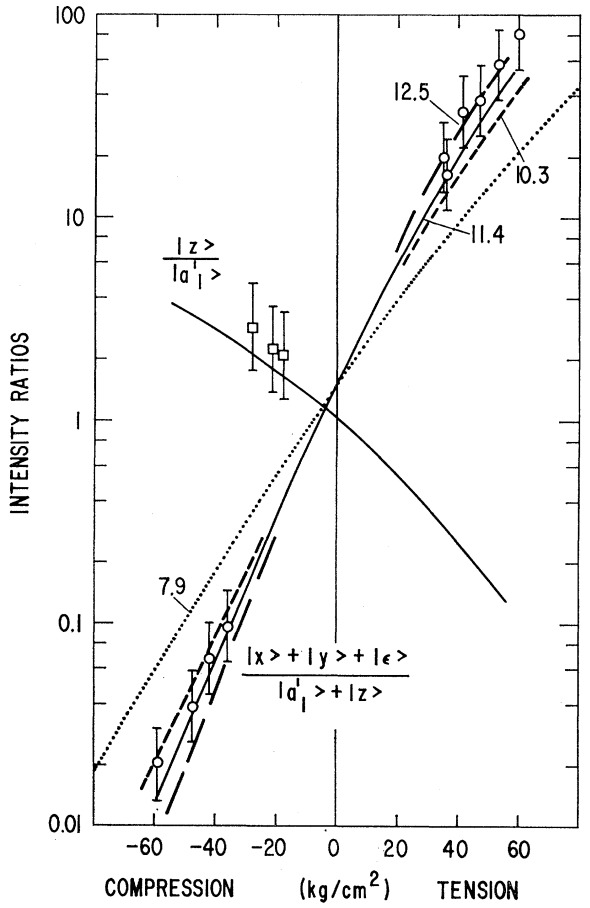

FIG. 18. Estimated integrated intensity ratios for the identified spectral lines versus [001] stress at $T=1.45$°K. The curves are calculated for different values of the deformation potential Ξ_u (indicated in eV).

obtain the result[55]

$$\delta E(T_2) = -\frac{\Xi_u^2}{30\pi^2\rho v_T^2}\left[1+\tfrac{2}{3}\left(\frac{v_T}{v_L}\right)^2\right]\int_0^\infty \frac{q^2\,dq}{[1+(\tfrac{1}{2}qa^*)^2]^4}$$
$$= -\frac{\Xi_u^2}{120\pi\rho a^{*3} v_T^2}\left[1+\tfrac{2}{3}\left(\frac{v_T}{v_L}\right)^2\right], \qquad (77)$$

where v_T and v_L are the sound velocities in the transverse and longitudinal branches of the acoustic phonon spectrum (which we have approximated as isotopic) and ρ is the crystal density. Substituting the appropriate values into Eq. (77), we obtain the very small value $\delta E(T_2) = -1.1$ cm^{-1}. For the doublet state E, if we omit the coupling with the excited vibronic states derived from the singlet electronic state A_1, we obtain in a similar manner a value for $\delta E(E)$ which is one-fourth of that for $\delta E(T_2)$. On the other hand, if we include the coupling to the states derived from A_1 and neglect the valley-orbit splitting between the singlet and doublet, we find $\delta E(E) = \delta E(A_1) = \delta E(T_2)$. The correct value for $\delta E(E)$ (obtained by including the valley-orbit splitting) will be between these values. We see, therefore, that these energy displacements as a result of the vibronic coupling contribute an energy difference of a fraction of 1 cm^{-1} between the E and T_2 states, with the triplet lower. This is, of course, a very small splitting, but it is clearly comparable with or possibly slightly larger than the splittings of the states ($\sim$0.1–0.2 cm^{-1}) due to residual strains which we inferred from our data. Since we concluded that the actual energy difference between the E and T_2 ground states of the lithium donor could not be appreciably larger than the strain splitting, we conclude that the electronic central-cell contribution to this difference must be of the same size and may in fact tend accidentally to cancel the predicted vibronic energy difference.

The valley-orbit splitting between the A_1 and E states results from an electronic central-cell effect since as we have noted, if we neglect this splitting, we calculate the same vibronic displacement for all three states. If this vibronic coupling were sufficiently strong, it would in fact tend to quench this electronic valley-orbit splitting, but in the present case this effect is negligible, the quenching factor being reduced from unity by less than 1%.[55]

We conclude, therefore, that these vibronic Jahn-Teller effects are too small for the lithium donor state (and for the other shallow donors in silicon as well), despite the degeneracy in its ground state, to have any practical importance in our interpretation of the EPR spectrum.

VII. STRESS DEPENDENCE OF SPECTRUM

A. g Shifts

In Fig. 14 and in Sec. VI A, we discussed in a qualitative way the effect of the level crossings as stress is applied and the resulting apparent divergences in the g values. Equation (69) can be used directly to give a quantitative expression for the effect for small stresses. The δ_{ij} can be expressed directly in terms of the applied stresses with the equations of Secs. III D and III E. From Eq. (69) we see that the g values are predicted to increase initially quadratically with applied stress, in general agreement with observation (Figs. 9 and 10).[56]

[55] Equation (77) follows directly from Eq. (4.2) of Ref. 10, while the calculation of the quenching factor for the valley-orbit splitting between the A_1 and E states follows from Eq. (4.3) of the same reference.

[56] The strong stress dependence of the effective g values found in Figs. 8–10 indicates that the spin-phonon coupling for the isolated lithium centers at low stress should be strong. This has been confirmed in ultrasonic attenuation measurements by J. K. Wigmore [Phys. Letters **26A**, 15 (1967)], using some of our samples, who has found a strong acoustic paramagnetic resonance absorption and has shown that the spin system can easily be saturated by the acoustic absorption under his experimental conditions.

B. Amplitudes versus Stress

The relative integrated intensities of the lines versus stress should reflect a Boltzmann distribution between the associated electronic states. Analysis of these intensities therefore allows us to check directly the energy-level diagram (Fig. 4).

In Fig. 9 we have labeled the electronic states associated with each of the prominent spectral lines in the transition region just beyond the crossover. The states T_2x, T_2y, $E\epsilon$, and T_2z have been discussed previously. The a_1' state, like the T_2z state, is made up mainly of z-directed valleys, and we anticipate that its g value should therefore follow closely that of the T_2z state. We therefore identify the weak shoulder shown in Fig. 9 on the T_2z state resonance under small compressional stress to be the line resulting from the a_1' state,[57] as indicated in Fig. 9. Elsewhere we assume these two lines to be unresolved.

In Fig. 18 we have plotted the relative integrated intensities of the various lines estimated from the recorded spectra versus stress at 1.45°K .The error bars indicate a rough estimate of the uncertainty of these determinations. The uncertainty is large because of the difficulty in separating the partially overlapping lines. However, because of the large range of stress over which the intensities can be followed, a sensitive check of the theory can still be made.

Using Eqs. (28)–(31) with $6\Delta_c=1.8$ meV to give the energies of the states, and equating the intensities to a Boltzmann distribution at $T=1.45$°K, we obtain the theoretical curves for several different assumed values of Ξ_u as shown in Fig. 18. The solid curves were calculated for $\Xi_u=11.4$ eV, which represents the best fit to the data. It can be seen that a good fit is possible, confirming the essential features of Fig. 4. The measured points for the intensity ratio z/a_1', though parallel to the predicted curve, appear $\sim 30\%$ high. This could be taken as evidence that the T_2 state is ~ 0.4°K (0.04 meV$=0.3$ cm^{-1}) below the E state in the unstressed crystal. However, this departure is within the estimated error, and we therefore cannot consider this significant.

From Fig. 18 we estimate

$$\Xi_u=11.4\pm 1.1 \text{ meV}. \tag{78}$$

This can be compared with the value 11 ± 1 eV estimated by Wilson and Feher[5] from stress dependence of the EPR for the substitutional donors. (To determine this value, Wilson and Feher were required to estimate the singlet-doublet energy separation for these donors indirectly. These energy separations have subsequently been measured directly by Aggarwal.[19] Reanalyzing Wilson and Feher's results using Aggarwal's values, we obtain for Ξ_u, 10.0 ± 0.6, 11.4 ± 0.7, and 11.3 ± 0.7 eV for phosphorus, arsenic, and anitmony, respectively. These are seen to be fully consistent with Wilson and Feher's original estimate.) Our result therefore agrees well with the estimate of Wilson and Feher.

On the other hand, significantly lower values seem to be indicated from other kinds of experiments. Krag *et al.*, for instance, have estimated 7.9 ± 0.2 eV from a direct study of the stress splitting of the infrared excitation spectra of sulfur[58] and phosphorus[59] donors. Similarly low values are found from cyclotron-resonance (8.5 ± 0.1 eV),[60] piezoresistance studies (8.3 ± 0.3 eV),[61] and piezooptic studies of the indirect absorption edge (8.6 ± 0.2 eV),[62] although these differ also from the Krag *et al.* value beyond their stated errors.

Figure 18 shows (dotted) the curve for Ξ_u of 7.9 eV, the value of Krag *et al.* This clearly does not fit our relative intensity data. To check this further, we have tried to fit the lithium ENDOR results using this value. A satisfactory fit can be made to the data of Fig. 12, while still requiring $6\Delta_c$ to be 1.80 meV.[63] The stress-dependence data of Fig. 13, however, cannot be fit very satisfactorily. This is shown as the dotted curve in Fig. 13. With this additional check, we are led to the tentative conclusion that the discrepancy is real. It does not appear possible to fit our data satisfactorily with such a low value for Ξ_u.

This large variation in the published estimates for Ξ_u has been previously pointed out by Aggarwal and Ramdas.[19] Superficially, it would appear that a different (larger) deformation potential is required to describe the interaction within the ground $1s$ manifold (Wilson and Feher's and our experiments) than that for excited bound states or for the conduction-band edge. However, the estimate of Schmidt-Tiedmann[64] from piezobirefringence studies of 11.3 ± 1.3 eV is an evident exception to this. This large variation between the results of different experiments remains to be explained.

VIII. SUMMARY

We have observed for the first time the EPR and ENDOR spectra of the shallow donor center due to an

[57] The resolution of the a_1' and z states puts a lower limit on the lifetime τ for each state. From the linewidths, we conclude $\tau\geq 3\times 10^{-8}$ sec. This is not inconsistent with the lifetime $\tau_{a'}\leq 2\times 10^{-7}$ sec inferred (at larger applied stress, however) from the lifetime averaging of the ENDOR spectrum.

[58] W. E. Krag, W. H. Kleiner, H. J. Zeiger, and S. Fischler, J. Phys. Soc. Japan Suppl. **21**, 230 (1966).

[59] W. E. Krag, M.I.T. Lincoln Laboratory, Solid State Research Report No. 4, 1967, p. 31 (unpublished).

[60] R. Ito, H. Kawamura, and M. Fukai, Phys. Letters **13**, 26 (1964).

[61] J. E. Aubrey, W. Gubler, T. Henningsen, and S. H. Koenig, Phys. Rev. **130**, 1667 (1963).

[62] I. Balslev, Phys. Rev. **143**, 636 (1966).

[63] With $\Xi_u=7.9$ eV and $6\Delta_c=1.8$ meV, the best fit to the data of Fig. 12 gives, using Eqs. (27), (29), (44), and (45) as before, $A_0/h=2.7$ Mc/sec. The value deduced for A_0 is therefore relatively insensitive to the value assumed for Ξ_u. In view of the uncertain state of Ξ_u, we have indicated in (46) an error for A_0/h of ± 0.5 Mc/sec, large enough to accommodate this estimate as well. Otherwise, with Ξ_u given by (78), the error estimate would be ± 0.3 Mc/sec.

[64] K. L. Schmidt-Tiedmann, in *Proceedings of the International Conference on the Physics of Semiconductors, Exeter, July, 1962* (The Institute of Physics and The Physical Society, London, 1962), p. 191.

isolated interstitial lithium atom in floating-zone silicon and our principal conclusions are the following:

(a) The conclusion of Aggarwal *et al.*[7] is confirmed that the valley-orbit splitting is inverted from the "normal" order.

(b) The doublet E and triplet T_2 comprising the ground state are accidentally degenerate, in the absence of any strain splitting, to within 0.1–0.2 cm^{-1} ($1–2\times10^{-5}$ eV).

(c) In zero applied stress the EPR spectrum below 2.5°K consists of a number of strongly anisotropic lines, the effective g factors of which are *all* larger than the values of $g_{\parallel}$ and $g_{\perp}$ for a single valley and exhibit a variation linear in H^{-2} [or ν_0^{-2}] when the experimental frequency is changed (the g values lie in the range 2.00–2.05 for $\nu_0=10$ KMc/sec). These g values are extremely sensitive to small applied stresses of order 1–10 kg/cm^2. Similar features are observed also in spectra taken with an applied stress that does not completely remove the fivefold orbital degeneracy of the ground state. These features are *not* accounted for by the independent-valley model.

(d) Under strong uniaxial compression along [001] or tension along [110] the ground state is T_2z, representing the antisymmetrical combination of valleys on the z axis, and the EPR spectrum is greatly simplified, agreeing now with the predictions of the independent-valley model. The single resonance has axial symmetry about [001], with $g_{\parallel}=1.9997\pm0.0001$, $g_{\perp}=1.9987\pm0.0001$, and the linewidth $\Delta H_{1/2}=1.3$ Oe is accounted for quantitatively on the basis of effective-mass theory by the Si^{29} hyperfine interaction.

(e) The general features of the zero-stress spectrum may be accounted for by postulating a weak spin-orbit interaction both among the T_2 states and between the E and T_2 states. Fitting the observed spectrum gives for the strength of the $E-T_2$ spin-orbit coupling the value $|\lambda'|\simeq0.056\,cm^{-1}$; the strength of the coupling among the T_2 states is less accurately determined because of uncertainties in the model but appears to lie in the range $|\lambda|\simeq0.01-0.02$ cm^{-1}. The splitting of the E and T_2 states as a result of random crystal strains must be postulated to be $>|\lambda|$, $|\lambda'|$, but $<g\beta H$. Typical strain splittings in the samples used must be 0.1–0.2 cm^{-1}, corresponding to rms residual strains $\langle e_\epsilon\rangle\sim\langle e_\theta\rangle\sim1-2\times10^{-6}$. Relaxation effects remain important in the doublet spectrum even at 1.5°K, and these are responsible for the changes in the spectrum that occur at higher temperatures.

(f) ENDOR spectra of Li^6, Li^7, and Si^{29} are observed from 1.3°K to ~4°K under strong compression along [001] and may be accounted for in terms of a lifetime-averaged hyperfine interaction of the T_2z ground state and the nearby excited state a_1'. The Li^7 hyperfine interaction is found to vary from $A/h\simeq0.01$ Mc/sec at 1.3°K to $A/h\simeq0.10$ Mc/sec at 4°K. This temperature variation shows that the Li hyperfine interaction in the ground state is very nearly zero, confirming that the T_2z state is the ground state under [001] compression, with its node at the (average) position of the Li. The small nonzero value $A_z/h\simeq0.004$ Mc/sec, inferred for the Li hyperfine interaction in the T_2z state by extrapolating to 0°K, is consistent with a theoretical estimate of the effect of zero-point vibrations of the Li ion in taking it out of the node if the Li local-mode frequency is ~500 cm^{-1}.

(g) The valley-orbit splitting $6\Delta_c$ between the doublet E and the (higher) singlet A_1 is determined from our data alone to be $6\Delta_c=1.8\pm0.3$ meV, thus confirming the value $6\Delta_c=1.8\pm0.1$ meV found by Aggarwal *et al.*[7]

(h) The Li hyperfine interaction in the excited singlet state in zero stress is determined from our data to be $A_0/h=2.3\pm0.5$ Mc/sec. This value corresponds to an enhancement factor $\eta_{Li}\simeq34$ in the electronic density at the Li nucleus, representing the correction to the predictions of simple effective-mass theory as a result of central-cell effects. This compares quite well with a theoretical estimate $\eta_{Li}\simeq49$ obtained simply by orthogonalizing the effective-mass wave function to the Li $1s$ core state.

(i) The EPR data show that the interstitial Li is definitely not in the hexagonal site but rather is in the tetrahedral site. While there is a possibility that the Li is displaced slightly out of the tetrahedral site, the evidence for this is not compelling.

(j) The small spin-orbit interaction among the triplet and doublet states results from the silicon spin-orbit interaction of the crystal and not from a residual effect of the Li atomic impurity.

(k) An analysis of the stress dependence of our EPR and ENDOR data leads to a value for the deformation potential parameter $\Xi_u=+11.4\pm1.1$ eV, which compares well with earlier determinations by Wilson and Feher[5] but less well with values obtained from optical experiments and some other studies.

ACKNOWLEDGMENT

The authors are grateful to Laura M. Roth, T. G. Castner, and A. K. Ramdas for helpful discussions of a number of points relating to this work. We are also grateful to Professor Ramdas for preparing the lithium-doped samples. We thank E. B. Tucker, Jr., R. Fedder, G. W. Ludwig, and H. H. Woodbury for the use of their EPR spectrometers at 10 and 14 kMc/sec. We thank also J. W. Corbett for making available to us a computer program for the line-shape calculations. W. Colliton assisted in all phases of the measurements.